This manuscript was published as formal in:

Ultrasonics – Sonochemistry 2018, 45, 238-247

DOI: 10.1016/10.1016/j.ultsonch.2018.03.022

https://doi.org/10.1016/j.ultsonch.2018.03.022

***Title*:**

Chiral betulin-imino-chitosan hydrogels by dynamic covalent sonochemistry

Manuela Maria Iftime, Luminita Marin*

[1] Petru Poni Institute of Macromolecular Chemistry of Romanian Academy, Iasi, Romania

*lmarin@icmpp.ro

Abstract

A series of chiral hydrogels was prepared from a homogeneous mixture of chitosan and betulinic aldehyde in different molar ratios, under the effect of ultrasound. The hydrogelation mechanism has been investigated by FTIR and CD spectroscopy, wide angle X-ray diffraction and polarized light microscopy. The morphology of hydrogels was examined by SEM. The swelling ability has been tested in three media of different pH. It was concluded that hydrogelation occurred by different pathways, closely related to the peculiarities of the chitosan-betulin systems. Circular dichroism measurements revealed chiroptical properties of the hydrogels, correlated to their content and crosslinking pathway.

Keywords: hydrogels, chitosan, betulin, dynamic covalent chemistry, chirality

1. Introduction

Biomaterials have been extensively studied in the last decades for their bio-applicability potential as implants, scaffolds for tissue engineering or matrix for targeted drug delivery, but also in other important domains as agriculture, environment protection, or food chemistry [1]. To this aim, natural compounds proved to be the most promising building blocks to create biomaterials due to their potential to preserve the biological properties and to mimic the natural tissues [2]. In this respect, our group developed a new strategy of hydrogelation of the chitosan biopolymer with monoaldehydes of natural provenience to provide hydrogels with eco-design [3-9]. The method is mainly based on the ability of the reversible imine units to self-order into clusters, which play the role of chitosan crosslinkers. In this way, using various aldehydes, biocompatible hydrogels with good mechanical properties [5,6], superporous morphology [7], antitumor activity [6], antifungal properties [8] or efficient luminescence [9] were obtained, paving the way to a new type of multifunctional hydrogels.

A class of natural compounds which lately attracted a lot of interest is that of chiral terpenes, due to their ability to fix biotargets and to induce special supramolecular architectures of the materials containing them [10,11]. An important representative is betulin – a triterpene which belongs to the lupane series and can be largely found in nature in the trees' bark, especially in the birch bark [12]. Its complex scaffold bearing eight asymmetric carbon atoms endows it with intrinsic chirality, an important advantage in chemoprevention and treatment of severe diseases, such as cancer and inflammations, due to the high affinity for stereospecific sites [13,14]. Moreover, the betulin chirality induces supramolecular architecturing of the compounds containing it making them important building blocks for designing optically active materials for biomedicine [15] and electro-optical devices [16].

Chitosan is one of the most abundant polysaccharides, studied for a large variety of bioapplications due to its impressive properties [1,17]. A less investigated property of the chitosan is its optical activity, which originates from the presence of the asymmetrically substituted carbon atoms which cause its helicoidal self-ordering while in solution [18-20]. The process is able to develop structural colors exploited in photonic materials to manipulate light [21], or to give chiral recognition harnessed in enantioseparation [22] or catalysis of enantioselective reactions [23]. The main difficulty in the synthesis of various chitosan derivatives is constituted by chitosan's low solubility. To overcome this drawback, recently, effect of ultrasound was used in the chemistry of chitosan, in the synthesis of block copolymers [24], chitosan capped copper nanoleaves [25], silver-chitosan nanoparticles [26], nanoparticles [27], nanovectors [28], nanoflakes [29], nanosheets [30] or nanofibers [31]. As can be seen, the use of sonication gave good results especially in the preparation of chitosan based nanoparticles, being envisaged that it had an important role in chitosan self-ordering. No reports regarding the preparation of chitosan hydrogels by sonication were found, despite the fact that the hydrogelation under the effect of ultrasound successfully worked for carbonaceous materials, coordination compounds, dendrons, organic low molecular weight compounds or polymers, and particularly for peptides [32-35]. The spontaneous aggregation under ultrasound stimuli was proposed as the main hydrogelation pathway, the potential self-assembling interactions (e.g. π-π stacking, H-bonds, van der Waals interactions, hydrophobic forces) playing a key role.

All these scientific achievements indicate that the combination of betulin with chitosan has good chances to accomplish a new biomaterial with great multifunctionality. Attempts to synthesize chitosan derivatives by reacting it with betulin indicated the avoidance of water as a favorable reaction parameter, but no information on the products properties were provided [36]. Under such circumstances, the aim of the paper was to obtain chitosan-betulin hydrogels. To this end, betulin was transformed into betulinic aldehyde, which was further reacted with chitosan polyamine to give chiral hydrogels. The key in obtaining the hydrogels was the use of effect of ultrasound which assured the system homogeneity, thus favoring the imination reaction and the supramolecular organization. The preparation of chitosan-betulin hydrogels and their chiroptical properties constitute the subject of this paper.

2. Experimental

2.1 Materials

Low molecular weight chitosan (217.74 kDa, 85 % deacetylation degree (DA)), betulin, Tempo reagent (98 %), sodium bicarbonate (99.7 %), sodium bromide (99.99), sodium

hypochlorite (99.9 %), sodium sulfite (98 %), magnesium sulphate (99 %), dichloromethane (99.8 %), ethanol 98 %, glacial acetic acid, acetone (99 %), hexane (99.5 %), ethyl acetate (99.8 %) and phosphate buffer solution of pH 7.4 were purchased from Sigma–Aldrich Co. (USA) and used as received. Acetate buffer solution of pH 4 was prepared in our laboratory, as already reported [5-9].

2.2 Synthesis

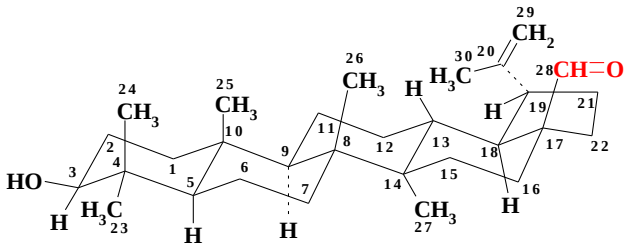

2.2.1 The synthesis of betulinic aldehyde was performed as per reported method [37], with some modifications, as follows. In a round bottom flask were introduced 0.0353 g Tempo reagent (1.13 mmol), 0.019 g $NaHCO_3$ (1.13 mmol), 0.0232 g NaBr (1.13 mmol) and 2 mL water to reach a concentration of the mixture of 3.875 %. The mixture has been vigorously stirred under nitrogen purge at room temperature for 5 minutes, and then, a solution of 0.1 g (1.13 mmol) betulin dissolved in 10 mL dichloromethane (1 %) was added. After 10 minutes stirring at room temperature, the reaction mixture was cooled down to 1 ^oC by immersing the flask in an ice bath, and then 4 mL of 0.5 % NaClO solution (1.13 mmol) was slowly dropped inside during 1 hour. The reaction mixture was kept for 4 hours at 1 ^oC, under vigorous stirring and inert atmosphere. After that, 2 mL of 0.5 % Na_2SO_3 solution was added and the mixture was further kept under stirring for 20 minutes. The two phases were separated in a separating funnel. The organic phase was firstly washed with brine solution and then with distilled water. The aqueous phase was extracted three times with dichloromethane (portions of 10 mL). The organic phase was dried on magnesium sulphate, filtered, and concentrated by rotary evaporation to give an orange viscous liquid. The crude product was purified by flash chromatography, using as eluent a mixture of hexane/ethylacetate 19/1. A white powder was obtained, which gave by recrystallization from methanol white needle crystals. η = 82 %, m.p. = 167-170 ^oC. **FTIR**, $\nu(cm^{-1})$: 1725 ($\nu_{C=O}$), 1642 ($\nu_{C=C}$); 883 ($\nu_{=CH2}$); **^{1}H-RMN**, δ(ppm): 9.66 (s, 1H, C<u>H</u>O); 4.74 (s, 1H, H29); 4.60 (s, 1H, H29); 4.27 (s, 1H, -O<u>H</u>); 2.97 (m, 1H, H3); 2.85 (m, 1H, H19); 2.01-0.99 (superposed peaks, 26H, C<u>H</u>, -C<u>H</u>$_2$, C<u>H</u>$_3$); 0.95 (s, 3H, H26); 0.86 (s, 3H, H25), 0.85 (s, 3H, H27); 0.77 (s, 3H, H23); 0.67 (m, 4H, H24, C<u>H</u>).

2.2.2 Hydrogel synthesis

Many trials involving the variation of the reaction conditions in terms of solvent (methanol, ethanol, acetone, dimethylsulfoxide), temperature, stirring type (magnetic, vortexing, ultrasonication) were necessary in order to establish the optimal conditions to reach hydrogels. Hydrogelation has been achieved when using the effect of ultrasound, at 55 ^{o}C, and the amount of water into the system was diminished by replacing it with ethanol, as follows.

In a 20 mL vial were introduced: 0,1 g chitosan ($5.05x10^{-4}$ mmol glucosamine units), 2.5 mL water, 2.5 mL ethanol and 35 µl glacial acetic acid, and stirred to give 2 % solution. Betulinic aldehyde was dissolved in ethanol to give a 1 % solution, which was heated at 55 ^{o}C before use. In order to obtain a series of hydrogels with different crosslinking density, different amounts of betulinic aldehyde were used, as given in Table 1. The vial containing the chitosan solution has been immersed in an ultrasonic bath, at 55 ^{o}C and ultrasonic frequency of 35 W. After 10 minutes, the solution of betulinic aldehyde was slowly dropped into the chitosan solution, (over 30-60 min, depending on the quantity of the aldehyde solution). While adding, at every 10 minutes, the vial was taken out from the ultrasonic bath and vigorously stirred on a vortex (1500 rot/min), in order to assure a better dispersion of the aldehyde into the viscous chitosan solution. In the case of the hydrogels with low amount of aldehyde, 1 mL of acetone has been added as co-solvent to preserve the system homogeneity. The reaction mixture transformed into an opalescent semisolid material after 3 hours, and became transparent after approx. 12 hours. The obtained products successfully passed the visual test of the inverted tube, once again confirming that they were hydrogels (Scheme 1).

Varying the ratio of amine/aldehyde functionalities, a series of 5 hydrogels was prepared (Table 1). The hydrogel samples were kept at room temperature for 1 week to remove the organic solvents, and after that were subjected to lyophilization in order to obtain the corresponding xerogels. A similar procedure was applied to a chitosan solution, to create a control sample. The molecular weight and DA degree of the ultrasonicated chitosan were determined and gave similar values with that of the parent chitosan (215.9 kDa, DA=85 %), showing that no other chemical modifications occurred during the sonication process.

Table 1. Hydrogel codes and their preparation conditions

Code	**CB0**	**CB2**	**CB2.5**	**CB3**	**CB5**	**CB6**
NH_2/CHO molar ratio	1:0	2:1	2.5:1	3:1	5:1	6:1
Chitosan/g	0.1	0.1	0.1	0.1	0.1	0.1
Glucosamine units/mol	$5.05x10^{-4}$	$5.05x10^{-4}$	$5.05x10^{-4}$	$5.05x10^{-4}$	$5.05x10^{-4}$	$5.05x10^{-4}$

Betulinic aldehyde/g	-	0.111	0.089	0.0742	0.044	0.037
Betulinic aldehyde/mol	-	$2.52x10^{-4}$	$2.02 x10^{-4}$	$1.68 x10^{-4}$	$1.01x10^{-4}$	$0.842x10^{-4}$
Ethanol/mL	2.5	11.1	8.9	7.4	4.45	3.71
Double distilled water/mL	2.5	2.5	2.5	2.5	2.5	2.5
Acetic acid/μL	35	35	35	35	35	35
Acetone/mL	-	-	1	-	1	1
Xerogel/g	0.098	0.209	0.189	0.174	0.143	0.137

Equipment

In order to analyze the structure and morphology of the hydrogels, the corresponding xerogels were obtained by freezing the hydrogels in liquid nitrogen and further submitting to lyophilization using a Bench Top Pro with Omnitronics ™ equipment, for 10 hours, at -55 ºC and 152 Pa.

Fourier-transform infrared (FTIR) spectroscopy has been performed on the ultrasonicated chitosan and the hydrogel lyophilized samples with a FT-IR Bruker Vertex 70 Spectrophotometer, by ATR technique. All spectra have been processed using OPUS 6.5 software.

Wide angle X-ray diffraction (WXRD) patterns were collected using a Bruker D8 Avance diffractometer with the Ni-filtered Cu-Kα radiation (λ = 0.1541 nm). The data were recorded on xerogel pellets, at 36 kV and 30 mA and the results were handled using FullProf 2000 software. The diffractograms were registered between 2-40^{o} (2 theta degrees). The pellets were obtained with a manual Hydraulic Press, by pressing at 10 N/m^{2}.

The textures of the samples and their thermotropic behavior were monitored on thin slices of hydrogels or xerogels, using an Olympus BH-2 polarized light microscope equipped with a THMS 600 heating stage and a LINKAM TP92 temperature control system.

The microstructure of the hydrogels was characterized by surface and cross-section viewing with a field emission Scanning Electron Microscope SEM EDAX – Quanta 200, operated at 20 keV accelerating voltage.

The swelling behavior was monitored by calculating mass equilibrium swelling (MES) with equation MES = (Ms-Md)/Md, where Ms is the mass of the hydrogel in swollen state and Md is the mass of the hydrogel in dried state. The measurements were performed in triplicate on square xerogels pieces, dried in advance in an oven, at 50 ºC, under vacuum. The data were

reported in mean values. Three different swelling media have been used: water, acetate buffer of acidic pH = 4.2 and phosphate buffer of basic pH = 7.4 (physiological pH). Shortly, the dry pieces of xerogels were immersed in swelling media, and taken out from time to time to be weighted, until no changes in their mass were observed. In order to establish their stability over time, the xerogels were kept in swelling media for three months.

The Circular dichroism (CD) spectra were acquired using a Chirascan plus (Applied Photophysics) by using 0.5 mm path lamellar cells. Far UV CD spectra were recorded from 280 to 190 nm with a step size of 0.5 nm and bandwidth of 1.5 nm. Near UV CD spectra were recorded from 400 to 250 nm a with step size of 0.5 nm and bandwidth of 1.5 nm. The measurements were performed at room temperature (22 ^{o}C).

3. Results and discussions

3.1 Hydrogel synthesis

A series of chiral hydrogels was obtained by reacting chitosan of low molecular weight with betulinic aldehyde, in different molar ratios of the amine/aldehyde functional groups (Table 1). The hydrogelation performed under the effect of ultrasound, which assured a proper balance between the homogeneity of the reaction system and the supramolecular architecturing. The formation of the hydrogels was hypothesized based on the fact that reversible forming of the imine bonds on chitosan chains favored the self-organization of the imine units in clusters, by imination and transimination processes (Scheme 1) [38]. These ordered clusters played the key role in hydrogelation, acting as unconventional crosslinking nodes of the chitosan chains [4-9]. Compared to other systems reported in literature, the betulinic aldehyde brings the feature of chirality, which keeps the promise to expand the functionality of the hydrogels to new opportunities of the biomaterials design. The hydrogelation of chitosan with betulinic aldehyde was a challenge due to the high hydrophobic character of the betulin triterpene, which facilitated its rapid crystallization in the aqueous solution of chitosan. To overcome this drawback, the amount of water into the system was diminished by replacing it with ethanol, the temperature was kept at 55 ^{o}C and the effect of ultrasound was employed.

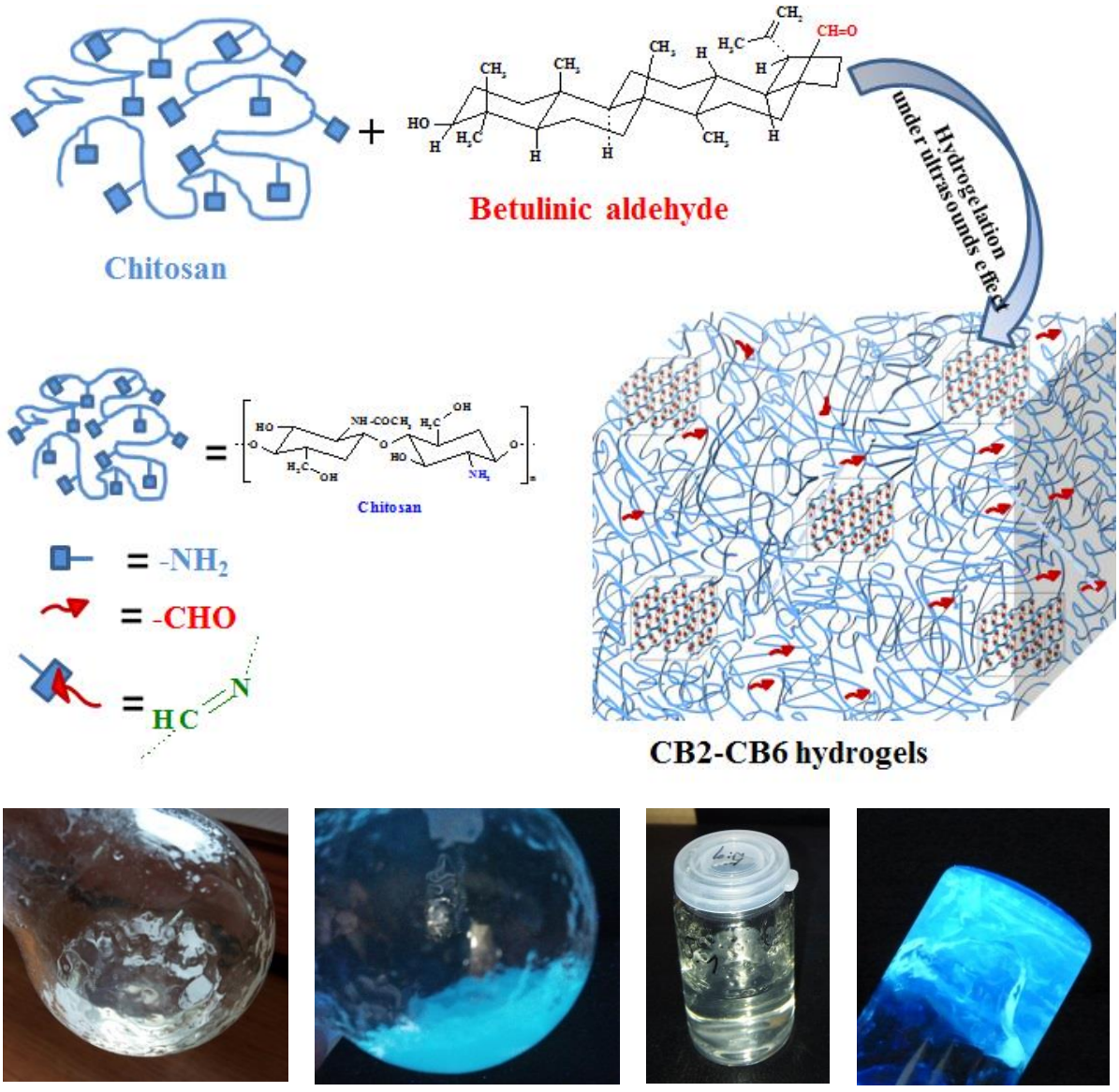

Scheme 1. Schematic representation of the chitosan hydrogelation with betulinic aldehyde and images of hydrogels under normal light and under illumination with an UV lamp

The hydrogels were transparent and emitted deep blue light when illuminated with an UV lamp (Scheme 1). To confirm the hydrogelation mechanism and further to understand their properties, the corresponding xerogels were analyzed by FTIR spectroscopy, X-ray diffraction, polarized light microscopy and circular dichroism spectroscopy.

3.2 FTIR spectroscopy

Studies on hydrogels obtained from chitosan and monoaldehydes revealed that hydrogelation was the result of the reversible formation of the imine units concomitant with their self-ordering in clusters which crosslink the chitosan chains; the imination being the trigger of the hydrogelation [4-9]. To establish to what extent the same hydrogelation

mechanism applied to the under study systems, FTIR spectra of the xerogels were analyzed in comparison with both chitosan and betulinic aldehyde precursors (Figure 1). Except the **CB3** sample, the vibration band of the betulinic aldehyde was still present in the xerogels spectra, around 1725 cm^{-1}. In the case of **CB3**, the aldehyde band almost vanished and a new band appeared at 1647 cm^{-1} – attributed to the stretching vibration of the imine bonds [5, 39]. The band had a medium intensity and overlapped with the band bearing to the vibration of the C=C linkage, at 1642 cm^{-1}.

A deeper view of the FTIR spectra by deconvolution of the fingerprint region revealed that the imine band was also present in the spectra of the other xerogels, but as a shoulder of lower intensity compared to the high intensity of the aldehyde band. This was surprising compared to the other imino-chitosan hydrogels, for which lyophilization entirely shifted the imination equilibrium to the products [4-9]. It was concluded that under the effect of ultrasound, the imination reaction and the self-ordering of the reagents were concurrent processes. Taking into consideration the reversibility of the imination, one could envision that an optimum molar ratio of the chitosan to the betulinic aldehyde guided a peculiar supramolecular architecturing by imination and transimination processes [18-20, 38, 40, 41].

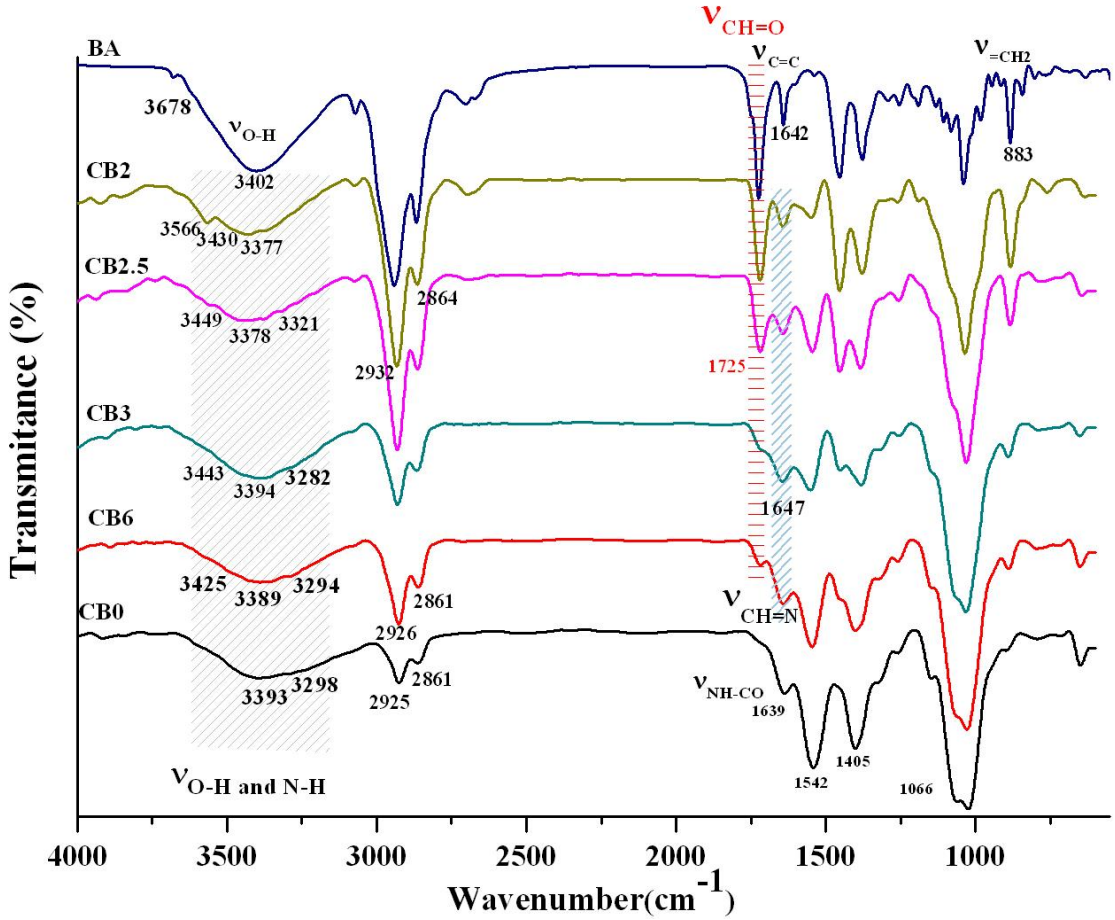

Figure 1. FTIR spectra of the xerogels and chitosan and betulinic aldehyde precursors

Modifications of the FTIR spectra could be seen in the 3700 - 2700 domain, associated with the stretching vibrations of the amine and hydroxyl groups involved in intra- and inter-molecular H-bonds [4, 42]. As usually, the chitosan showed in this region two broad overlapped bands, at 3393 and 3298 cm^{-1}, attributed to the presence of the intra- and inter-molecular H-bonds, respectively [42, 43]. The betulinic aldehyde showed a broad band with a maximum at 3402 cm^{-1}. The xerogel samples exhibited slight shifting of the two overlapped bands to higher or lower wavenumbers and the appearance of a new vibration band around 3566 cm^{-1} attributed to the modification of the H-bonding network, according to new interactions inside the chitosan/betulinic aldehyde systems [43]. This comes in line with the use of effect of ultrasound, which favors physical interactions [32-36].

Thus, the FTIR data suggested that sonication favored the occurrence of chemical and/or physical interactions, whose dominance depended on the molar ratio of the hydrogel components.

This hypothesis was supported by (i) the decreased reactivity of the aldehyde group because of steric hindrance of the betulin skeleton and (ii) the presence of the hydroxyl group and hydrogen atoms in equatorial positions on the betulin, which are more susceptible to H-bonds formation [44]. It must be considered that both chemical and physical processes were influenced by the ultrasonic treatment [25-35]. Moreover, the antagonistic nature of the two reagents: hydrophobic betulinic aldehyde and hydrophilic chitosan should have a significant influence on the supramolecular ordering of the system, too [5].

3.3 Supramolecular ordering of the hydrogels

To further understand the gelling mechanism of the chitosan - betulinic aldehyde system under the effect of ultrasound, the peculiarities of the supramolecular ordering were analyzed comparing the wide angle X-ray diffraction patterns of the ultrasonicated chitosan (**CB0**), betulinic aldehyde and xerogels based on them (Figure 2).

Firstly, it is important to notice the drastic change of the chitosan morphology under the effect of ultrasound (Figure 2a). Usually, the chitosan as film, powder or lyophilized sponge – showed two broad superposed bands with maxima around 22 ^{o} and 12 ^{o}, attributed to the intramolecular (4.1 Å) and intermolecular d-spacing (7.4 Å), of the ordered domains (dry chitosan) dispersed into amorphous domains (hydrated chitosan) [43]. The crystallinity degree results from the ratio of the two domains. As can be seen in figure 2a, the ultrasonicated chitosan showed drastic changes of the diffractogram consisting in the splitting of each broad band in two sharper peaks, indicating a considerable increase of the crystallinity. Taking into

consideration the previous studies on chitosan structure and its supramolecular organization, the changes were attributed to the increasing of the density of the intra-molecular H-bonds which led to the growing the ordered domains to the detriment of the amorphous ones [1].

The diffraction pattern of the betulinic aldehyde (Figure 2c) revealed two principal reflections in a smaller angular domain, at 5.97 º and 6.77 º, correlated with the inter-layer distance (14.8 Å and 13.07 Å, respectively), and many reflections in wide angle domain around 14.62 º, correlated with the inter-molecular distances given by H-bonds and betulin-betulin hydrophobic interactions (around 6.1 Å). According to this diffraction pattern, the driving force of the supramolecular organization of the betulinic aldehyde appeared to be the H-bonding and hydrophobic-hydrophobic interactions between the betulin skeleton units.

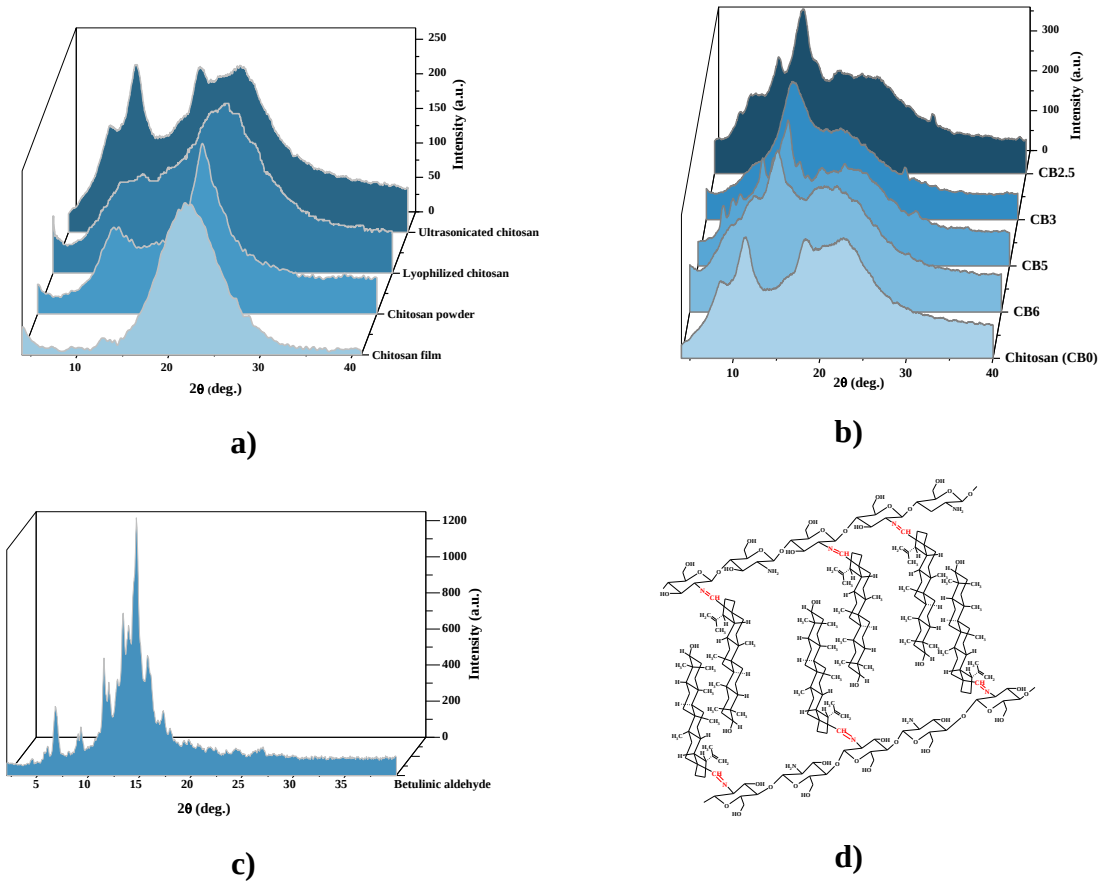

Figure 2. X-ray diffraction of a) chitosan as powder, processed as film, and lyophilized sponge, with or without ultrasound treatment; b) ultrasonicated chitosan and studied **CB2.5-CB6** xerogels; c) betulinic aldehyde; and d) model of the supramolecular architecturing of betulin-imino-chitosan units

Looking at the diffraction pattern of the xerogels, features of both chitosan and betulin skeleton profiles could be retrieved, in different proportions, indicating different influences of

their ordering driving forces upon the xerogel architectures (Figure 2b). The **CB3** distinguished itself by a different diffractogram compared to the other xerogels. Features of the X-ray diffractograms are as follows: (i) All the xerogels showed an intense reflection around 14.2 °, corresponding to a d-spacing of 6.2 Å, close to the inter-molecular distances of betulin. (ii) Except **CB3**, the other xerogels showed also sharper reflections attributed to the intrinsic ordering of the betulin and chitosan. Their absence in the **CB3** diffractogram was correlated with its higher imination ratio (as demonstrated by FTIR), which favored a more homogeneous supramolecular architecturing of the betulin-imino-chitosan units (Figure 2d) (iii) The sharp reflections in ultrasonicated chitosan diffractogram diminished in intensity and almost disappeared for **CB3** xerogel. This indicated the disruption of the intra- and inter-molecular H-bonds of chitosan, in agreement with the presence of the bulky betulin which favored new intermolecular interactions. (iv) The appearance of a new reflection in wide angle domain (26 °, for **CB3** and 29 ° for the others), corresponding to small intermolecular distances of 3.5 Å and 3.1 Å, respectively, which was attributed to the formation of the H-bonds between the newly formed imine units. The occurrence of these new bonds hindered the betulin mobility constraining it to closer interactions (Figure 2d). (v) All reflections in the xerogels diffractograms were broader compared to those of their precursors, indicating a polydispersity of the d-spacings, characteristic to the semicrystalline systems [45-47], in agreement with the formation of ordered clusters bonding amorphous domains of chitosan (Scheme 1).

X-ray data confirmed that the hydrogelation of the chitosan-betulinic aldehyde systems was a direct consequence of the self-ordering of the betulin skeleton, either grafted to the chitosan chains by covalent imine bonds or by physical forces. Correlating FTIR and X-ray diffraction measurements, it appeared that the hydrogelation was driven by the competition of the chemical/physical forces under the effect of ultrasound, which generated ordered supramolecular clusters linking the chitosan chains.

3.4 Polarized light microscopy (POM)

It is well known that ordered materials show birefringent textures under polarized light due to their optical anisotropy. The texture appearance is correlated to the specific features of the supramolecular arrangement and is useful in determining the ordering type [48].

Literature data revealed that chitosan chains in solution self-ordered for a critical concentration value forming a chiral lyotropic liquid crystal [18-20, 49]. It was observed that in the case of the substituted chitosan, the critical concentration increased as the length of the lateral chain increased. As an example, chitosan grafted with cholesterol gave chiral lyotropic

liquid crystals in organic solvents, with characteristic textures [50]. In this light, the observation of the textures of the studied hydrogels and their precursors was expected to provide information regarding the type of supramolecular organization and the driving forces to reach it.

As can be seen in figure 3, the ultrasonicated chitosan (**CB0**) exhibited a fine Schlieren texture, similar to those observed for rigid or semiflexible polymers which have ordering difficulties in molten state [46, 51]. This was in agreement with the increased crystallinity of the ultrasonicated chitosan, as demonstrated by X-ray measurements. The betulinic aldehyde showed a marble texture with vivid colors, in agreement with its three-dimensional ordering.

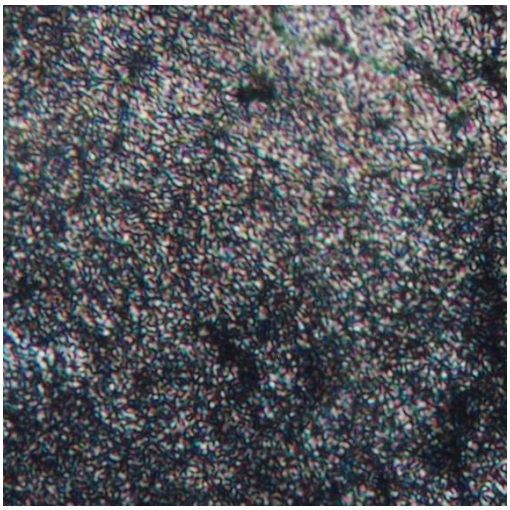

CB0, xerogel

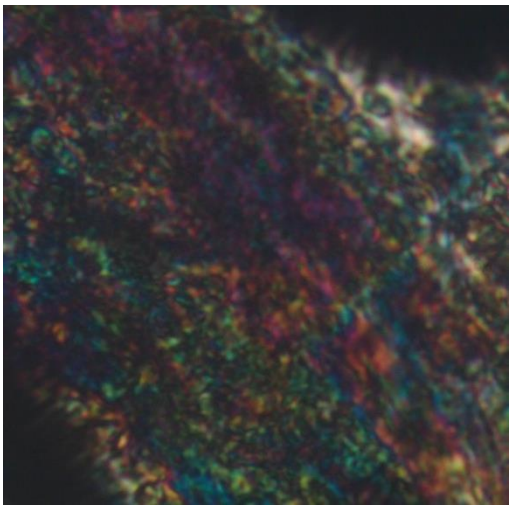

Betulinic aldehyde

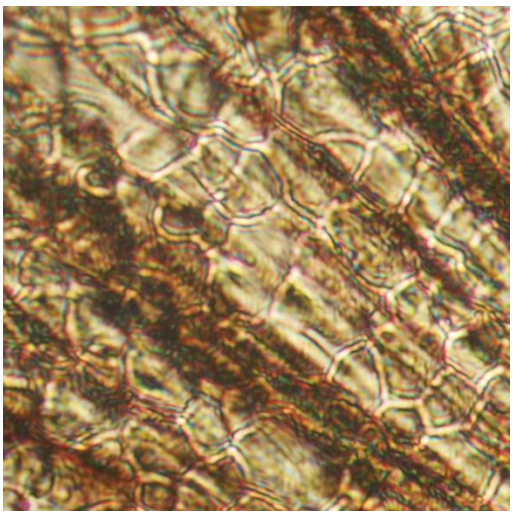

CB2 xerogel

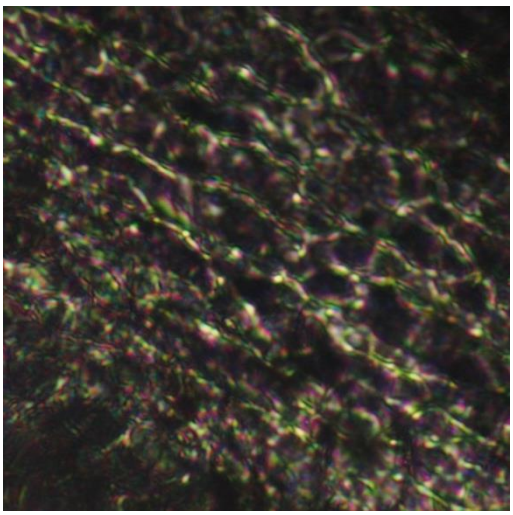

CB2.5 xerogel

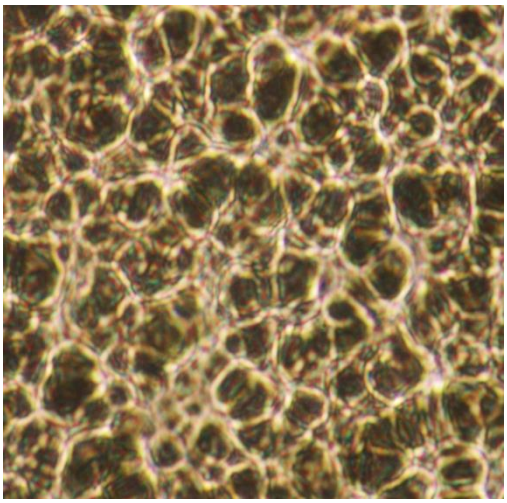

CB3 hydrogel

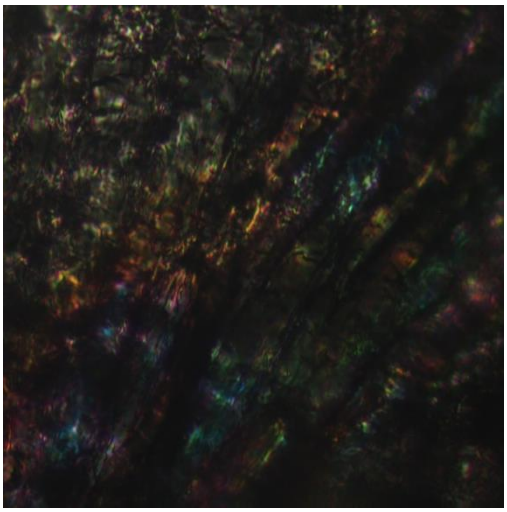

CB3 hydrogel, thin film

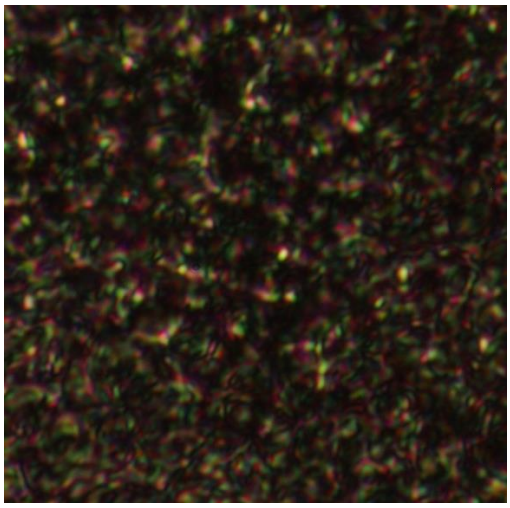

CB5 xerogel

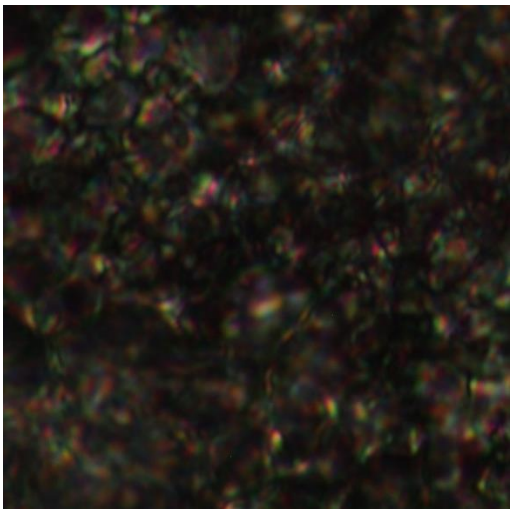

CB6 xerogel

Figure 3. POM microphotographs acquired at room temperature and magnification of 200x

The **CB2-CB6** xerogels presented oily-streak lines, characteristic for a helical organization of long pitch helix with network-like defect lines, suggesting that chitosan – betulinic aldehyde systems formed a cholesteric lyotropic mesophase into the solution state [52]. Moreover, the texture of the **CB3** sample in thin film developed into a fingerprint pattern with Grandjean-Cano lines, characteristic to a helical structure of short pitch, typical to a cholesteric liquid crystal arrangement with comparatively longer helical periodicity. Both textures belong to a chiral nematic mesophase. Compared to the texture of chitosan, those of the hydrogels/xerogels were clearer, with more vivid colors, signature of a more ordered material. They were homogeneous, without segregated domains indicating an intimate mixing of the chitosan and betulinic aldehyde into a network, either by forming covalent imine units or physical bonds. Comparing the texture of the **CB3** to the other hydrogels/xerogels, a significant

influence of the covalent bonding on the supramolecular organization was apparent. This resulted in a more homogeneous dispersity of the helix pitch. It could be concluded that bonding of the betulinic aldehyde to chitosan, either by covalent or physical bonds favored a cholesteric ordering which led to lyotropic hydrogels.

The sample textures remained unaffected by heating up to 140 ^{o}C, and showed progressive browning as the temperature increased further, according to the occurrence of thermal degradation of the chitosan [53].

Moreover, the observation of the xerogels samples swollen in three media of different pH (4.2, 7, 7.4) didn't reveal significant changes, pointing for a good stability of the cholesteric mesophase in solutions of different pH.

3.5 Hydrogel microstructure

The microstructure of the hydrogels was investigated by scanning electron microscopy on the corresponding xerogels samples (Figure 4). Comparing the SEM images with the X-ray diffractograms, a correlation between nanostructure and microstructure was evident.

The ultrasonicated chitosan yielded by lyophilization a film with rare, small pores, with diameter between 4 - 7 µm. This microstructure is related with its higher degree of crystallinity employing an H-bonding network of the hydroxyl groups, making them less available for H-bonds with water molecules, and thus hindering the entrapping of large amounts of water.

The **CB3** hydrogel**,** characterized by predominant covalent bonding of the betulinic aldehyde to chitosan, showed a typical microporous morphology with interconnected, micrometric pores around 10 µm. A microporous morphology was also evident in the case of **CB6** hydrogel incorporating the smallest amount of betulinic aldehyde. In the last case, the pores were denser, with even smaller diameter, around 5 µm. Looking at the XRD diffractograms of the two xerogels, a quite similar diffraction pattern could be seen, with the predominance of the reflection characteristic to the intermolecular distances between betulin skeletons.

The other hydrogels showed a network of entangled micro- and nano-fibers, whose diameter decreases as the amount of betulinic aldehyde into hydrogel decreased, from 5 µm (**CB2**) up to 1 µm (**CB5**). In the case of **CB2** sample, the entanglement of the fibers formed pores of diameter between 10-50 µm, while in the case of the other xerogels, the fibers formed a dense fibrillar network.

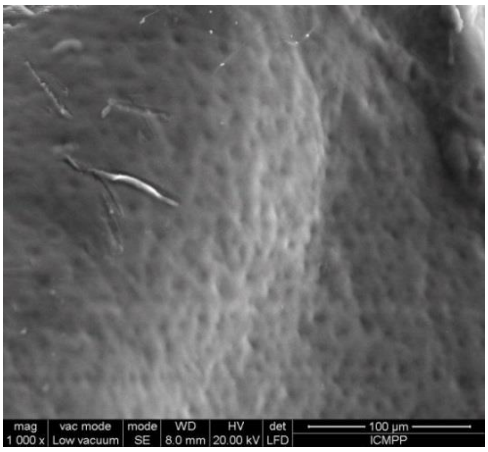

CB0

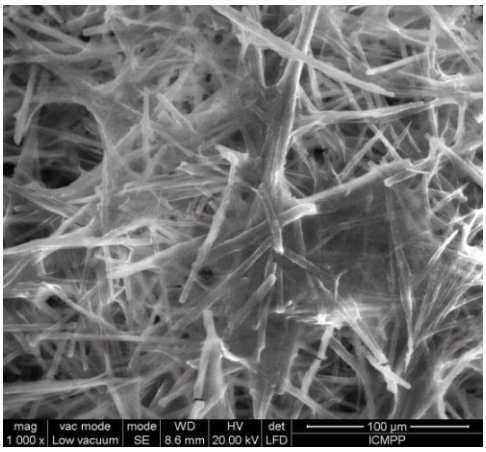

CB2

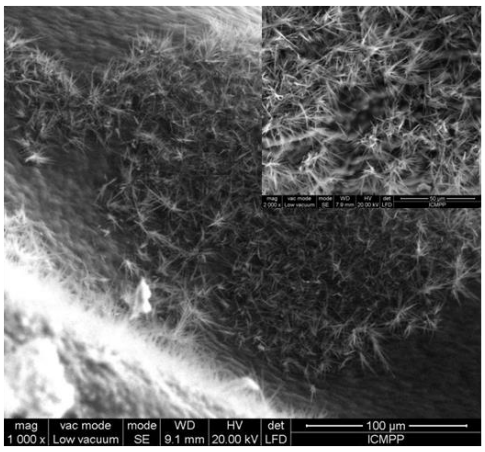

CB2.5

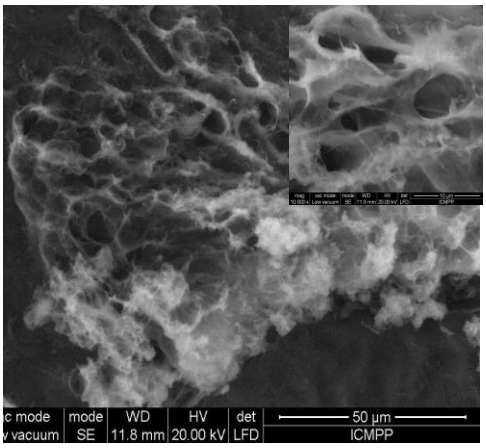

CB3

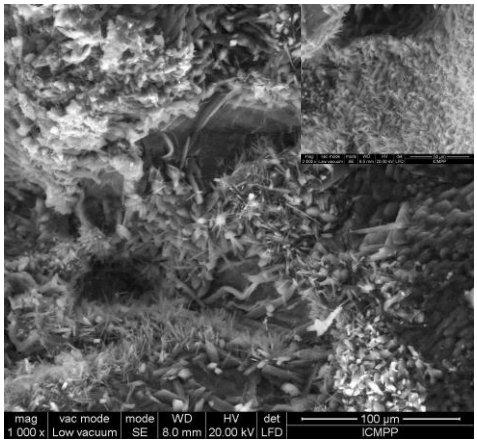

CB5

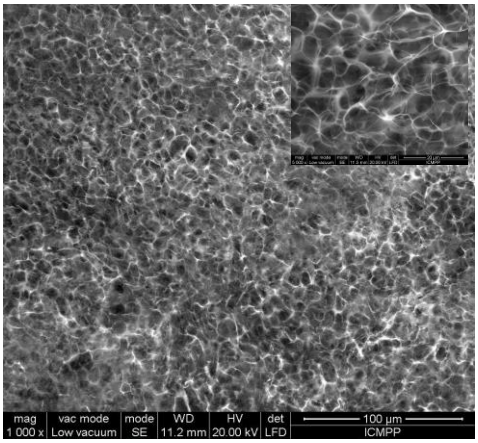

CB6

Figure 4. SEM microphotographs of **CB0** ultrasonicated chitosan and **CB2**-**CB6** xerogels

3.6 Swelling behavior

Generally speaking, the swelling behavior of chitosan hydrogels is related to their crosslinking nature and it is an important parameter which defines their application; those physically crosslinked suffer a rapid dissolution, while those chemically crosslinked are more

stable in swelling media and consequently more appropriate for *in vivo* applications [6,7]. The swelling behavior was investigated on xerogels, by measuring the mass equilibrium swelling (MES) in three media of different pH: phosphate buffer of physiological pH (7.4), acetate buffer of acidic pH (4.2) and water of neutral pH (7). In all three media the xerogels completely rehydrated generating the initial hydrogels (Figure 5). The MES was rapidly reached in 10 minutes in water and acetate buffer and slowly, in 3 hours, in phosphate buffer. In acetate buffer the swelling competed with the dissolution, which was completed after 3 weeks. In water and phosphate buffer the hydrogels were more stable; those with higher content of aldehyde (**CB2**, **CB2.5**, **CB3**) kept their integrity even over 3 months, while those with lower aldehyde content dissolved in one month.

The MES value was related to the content of aldehyde, its bonding to chitosan (covalent or physical) and pH of the swelling media. An increasing trend of MES along with decreasing of the betulinic aldehyde content was registered in all three media, with a deviation in the case of **CB3** with dominant covalent bonding (Figure 5). In neutral media the MES varied from 18 to 69, while in phosphate buffer from 8 to 18. In phosphate buffer of physiological pH the hydrogels showed excellent shape preservation, the MES being in fact the result of filling the pores with molecules of the swelling media. This presents a particular interest for tissue engineering which requires dimensional stability in physiological pH [54].

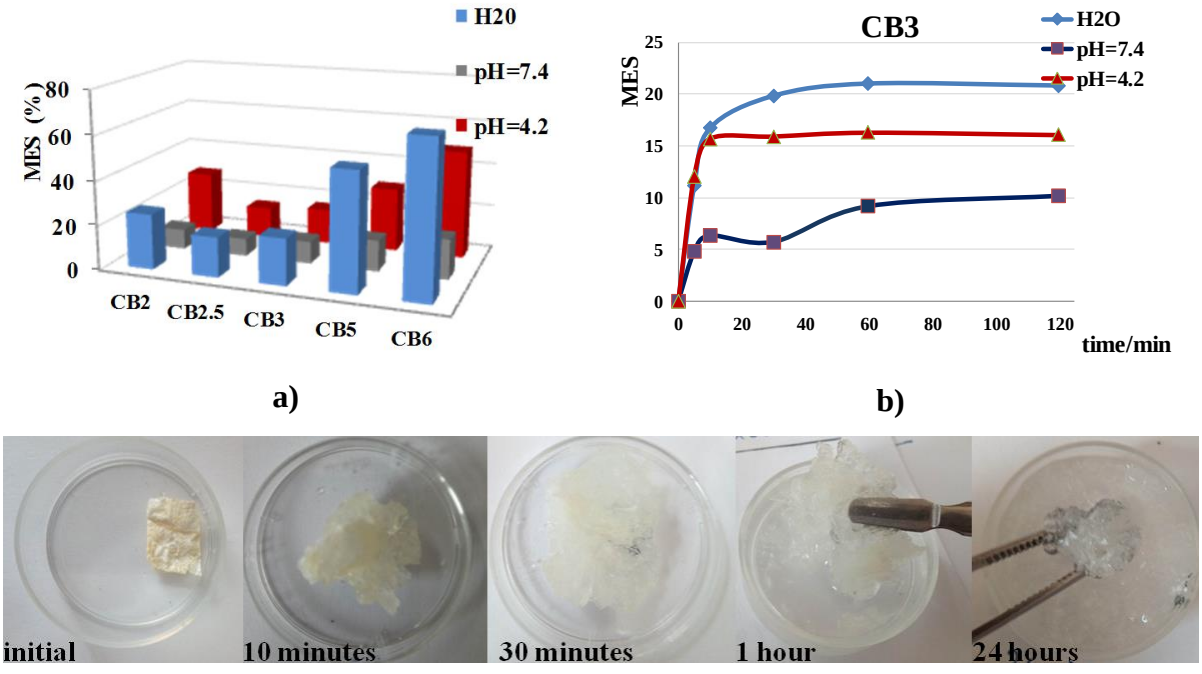

Figure 5. a) Mass equilibrium swelling in different pH media of the **a)** hydrogels and **b) CB3** measured during the time and c) images of hydrogel **CB2** before and after swelling in water

3.7 Circular dichroism spectroscopy

Chiroptical properties of the hydrogels were investigated by circular dichroism (CD) spectroscopy, comparing them with those of chitosan and betulinic aldehyde precursors. It is known that the CD profile is closely related to the chiral supramolecular architecture of the material, allowing the estimation of the supramolecular changes during hydrogelation [55]. As can be seen in figure 6, the betulinic aldehyde showed three bands in far-UV domain, with maxima at 198, 205 and 223 nm and a band in near-UV at 322 nm. The bands in the far-UV originated from the n-π* transitions in carbonyl group of saturated polycyclic hexanone structure located in an ordered, regular arrangement. The band in near-UV indicated a three dimensional arrangement of the betulinic aldehyde, attributed to a helical architecture due to its asymmetrical carbon atoms. The negative band following the positive bands indicates R and S configurations [56]. Chitosan presented a well-defined negative band in far-UV spectral region at 220 nm with a left-shoulder at 204 nm and a positive band in near-UV domain around 260 nm, also observed for chitosan films [57]. The negative band was attributed to the electronic transitions in the amide groups, while the positive band corresponded to the n-π* transitions in the amine groups. The lower intensity of the positive band compared to the negative one was due to the transformation of the amine groups into salts during solubilization in the acidic solution. The occurrence of the bands in the CD spectra indicated that the amide and amine groups on chitosan were located in well-defined structures, attributed to a two-fold helix stabilized by intra-molecular H-bonds [58].

Looking at the shape of the CD spectra of the hydrogels, a different profile could be seen, depending on the content of betulin and the crosslinking pathway. Thus, the **CB5** and **CB6** hydrogels, containing the lowest betulin amount, mostly linked to chitosan by physical interactions, showed absorption bands quite similar to that of chitosan, with a negative band at 218 and 213 nm, respectively, with a right-shoulder at 241 and 249 nm respectively, and a low intense positive band around 270 nm. This indicated the dominance of the self-ordering of chitosan as driving force of the hydrogelation process. The small differences, consisting in the left-shifting of the negative band, disappearance of the left-shoulder and the occurrence of a right-shoulder, indicated modifications of the arrangement of the amide groups into arrays, possibly prompted by the H-bonding with betulin skeleton. No differences in the positive band were registered, indicating no implication of the amine groups into physical interactions with betulin. The presence of the negative and positive bands showed the presence of two enantiomer forms.

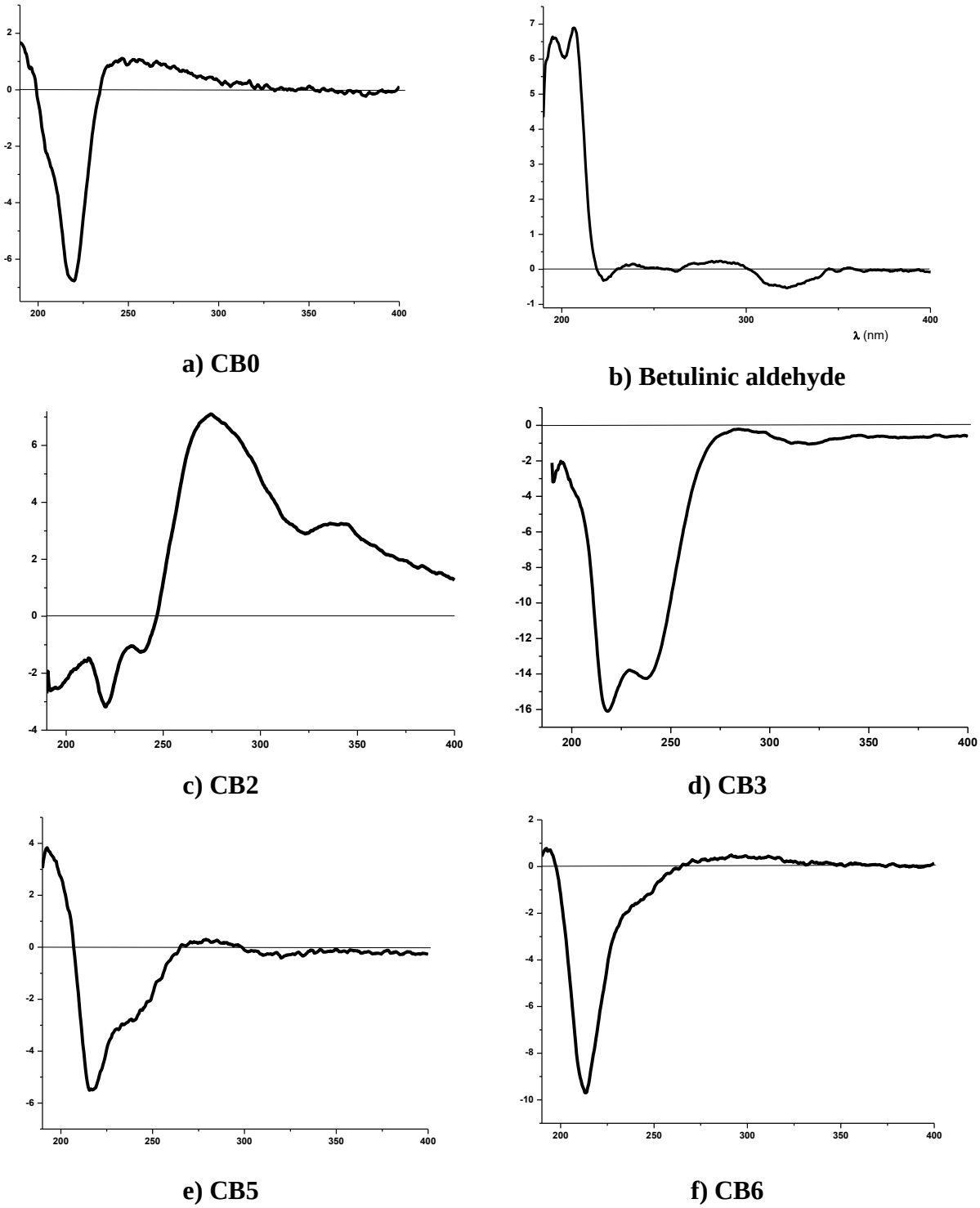

Figure 6. Circular dichroism spectra of the studied hydrogels and their precursors

By comparison, the **CB3** hydrogel exhibited the negative optical transition in the far-UV splitted in well-defined bands at 191, 218 and 238 nm, while in the near-UV domain a new negative band appeared around 319 nm. This major transformation of the CD spectrum indicated a complete different pattern of supramolecular ordering. The negative band around

319 nm was attributed to the appearance of the R enantiomer of the chiral imine chromophore [59]. The splitting of the negative band into multiple transitions was ascribed to the formation of ordered arrays of the newly formed imine units. Remarkably, the absorption occurred entirely in the negative region, indicating the dominance of the right-handed configuration.

The **CB2** hydrogel with the highest amount of betulinic aldehyde, also showed the multiple transitions into the negative far-UV region at 192, 220, 239 nm characteristic to the formation of ordered arrays of amide/imine units. By contrast, the hydrogel exhibited two intense bands at 280 and 340 nm in the positive near-UV region, in line with the formation of betulin arrays, as SEM indicated. The presence of negative and positive absorption bands confirms both R and S configurations.

Compared to the CD spectrum of betulinic aldehyde, the CD spectra of the hydrogels showed a Cotton effect indicating that a chirality inversion took place during hydrogelation. This was attributed to the cholesteric supramolecular ordering which occurred during hydrogelation, producing a different handed configuration, as was also observed for the hydrogelation of peptides [35].

Thus, the CD spectra of the hydrogels clearly revealed their supramolecular chirality due to a three-dimensional arrangement generated by the asymmetrical carbon atoms of chitosan and betulin skeleton, physically or chemically bonded. This assessment fully supported the conclusions of FTIR, X-ray and POM measurements, reinforcing the idea that hydrogelation was driven by the supramolecular ordering. Moreover, the circular dichroism measurements brought supplementary data, confirming the POM suppositions that chiral atoms in betulin and chitosan underpin a cholesteric supramolecular ordering leading to a supramolecular chirality.

Conclusions

Chiral hydrogels were successfully prepared from chitosan polyamine and betulinic aldehyde under the effect of ultrasound. Comparing data of FTIR and CD spectroscopy, X-ray diffraction and polarized light microscopy, it was concluded that the driving force of hydrogelation was the supramolecular chiral architecturing of the betulin skeleton into ordered clusters. The ultrasonication assured a proper balance between the system homogeneity and supramolecular ordering which led to the formation of clear transparent hydrogels. The ordering process has been favored by the dynamic bonding of betulin to the chitosan chains by physical forces or reversible covalent imine linkages. The ordered clusters play the role of atypical crosslinking nodes of the chitosan chains into a hydrogel network. The hydrogels have a microporous or entangled fibrous morphology, closely related to the physical or covalent

bonding of betulin to chitosan. They swollen well in acidic and neutral media and preserved their shape in basic medium of physiological pH. Despite the dynamic bonding, the ordered clusters were robust enough to endow hydrogels with good stability in all three swelling media. The hydrogels showed chiroptical properties, and homochirality when betulin was covalently bonded to chitosan.

These results proved a novel pathway towards chiral hydrogels with eco-design based on chitosan biopolymer, indicating a new approach of exploiting chitosan in medical and pharmaceutical applications.

Acknowledgements

The financial support through Romanian National Authority for Scientific Research MEN – UEFISCDI grant, project number PN-II-RU-TE-2014-4-2314 and through the European Union's Horizon 2020 research and innovation programme under grant agreement 667387 is highly acknowledged.

The authors are thankful to Professor Mihai Barboiu, Institut Européen des Membranes, Montpellier, France for useful discussions related to the dynamic covalent chemistry.

References

References

[1] M. Rinaudo, Chitin and chitosan: Properties and applications, Prog. Polym. Sci. 31 (2006) 603-632.

[2] I.G. Beskardes, T.T. Demirtas, M.D. Durukan, M. Gumusderelioglu, Microwave assisted fabrication of chitosan hydroxyapatite superporous hydrogel composites as bone scaffolds, J. Tissue. Eng. Regen. Med. 9 (2015) 1233-1246.

[3] L. Marin, B. C. Simionescu, M. Barboiu, Imino-chitosan biodynamers, Chem. Commun. 48 (2012) 8778-8780.

[4] L. Marin, S. Morariu, M. C. Popescu, A. Nicolescu, C. Zgardan, B. C. Simionescu, M. Barboiu, Out-of-water constitutional self-organization of chitosan–cinnamaldehyde dynagels, Chem. Eur. J. 20 (2014) 4814-4821.

[5] L. Marin, D. Ailincai, S. Morariu, L. Tartau-Mititelu, Development of biocompatible glycodynameric hydrogels joining two natural motifs by dynamic constitutional chemistry, Carbohydr. Polym. 170 (2017) 60-71.

[6] A.M. Olaru, L. Marin, S. Morariu, G. Pricope, M. Pinteala, L. Tartau-Mititelu, Biocompatible chitosan based hydrogels for potential application in local tumour therapy, Carbohydr. Polym. 179 (2018) 59-70.

[7] M. Iftime, S. Morariu, L. Marin, Salicyl-imine-chitosan hydrogels: supramolecular architecturing as a crosslinking method toward multifunctional hydrogels, Carbohydr. Polym. 165 (2017) 39-50.

[8] D. Ailincai, L. Marin, S. Morariu, M. Mares, A.C., Bostanaru, M. Pinteala, B.C. Simionescu, M. Barboiu, Dual crosslinked iminoboronate-chitosan hydrogels with strong antifungal activity against Candida planktonic yeasts and biofilms, Carbohydr. Polym. 152 (2016) 306-316.

[9] A. Bejan, D. Ailincai, B. C. Simionescu, L. Marin - Chitosan hydrogelation with a phenothiazine based aldehyde – toward highly luminescent biomaterials, Polym. Chem. (2018) doi: 10.1039/C7PY01678F.

[10] B. Singh, R.A. Sharma, Plant terpenes: defense responses, phylogenetic analysis, regulation and clinical applications, Biotech. 5 (2015) 129-151.

[11] T.J. Maimone, P. S Baran, Modern synthetic efforts toward biologically active terpenes, Nat. Chem. Biol. 3 (2007) 396-407.

[12] J.D. Connolly Robert, A. Hill, Triterpenoids, Nat. Prod. Rep. 27 (2010) 79-132.

[13] N.K.R. Pathak, P. Neogi, M. R. Biswas, V.B. Pandey, Betulin aldehyde, an antitumour agent from the bark of Tectona grandis, Indian J. Pharm Sci. 50 (1988)124-125.

[14] S. Haque, D.A. Nawrot, S. Alakurtti, L. Ghemtio, J. Yli-Kauhaluoma, P. Tammela, Screening and characterisation of antimicrobial properties of semisynthetic betulin derivatives, Plos One 9 (2014) e102696.

[15] M. Mitov, Cholesteric liquid crystals in living matter, Soft Matter 13 (2017) 4176-4209.

[16] S.H. Kim, L.-C. Chien, Short pitch cholesteric electro-optical device stabilized by non-uniform polymer network, Appl. Phys. Lett. 86 (2005) 161118.

[17] V. Zargar, M. Asghari, A. Dashti, A review on chitin and chitosan polymers: structure, chemistry, solubility, derivatives, and applications, Chem. Bio. Eng. Reviews 2 (2015) 204-226.

[18] Y. Dong, Y. Wu, Y. Zhao, H. Wang, Y. Ruan, H. Zhang, X. Fang, Change of handedness in cholesteric liquid crystalline phase for N-phthaloylchitosan solutions in organic solvents, Carbohydr. Res. 338 (2003) 1699-1705.

[19] S.B. Murray, A.C. Neville, The role of pH, temperature and nucleation in the formation of cholesteric liquid crystal spherulites from chitin and chitosan, Internat. J. Biolog. Macromol. 22 (1998) 137-144.

[20] Y. Dong, Q. Yuan, Y. Huang, Textures and disclinations in the cholesteric liquid crystalline phase of a cyanoethyl chitosan solution, J. Polym. Sci., Part B: Polym. Phys. 38 (2000) 980-986.

[21] T.-D. Nguyen, B.U. Peres, M.R. Carvalho, M.J. MacLachlan, Photonic hydrogels from chiral nematic mesoporous chitosan nanofibril assemblies, Adv. Funct. Mater. 26 (2016) 2875-2881.

[22] J. Wang, J.B. Xi, W. Chen, S.H. Huang, Z.W. Bai, High performance chiral separation materials based on chitosan bis(3,5-dimethylphenylcarbamate)-(alhyl urea)s, Carbohydr. Polym. 156 (2017) 481-589.

[23] A.E. Kadib, Chitosan as a sustainable organocatalyst: a concise overview, "ChemSusChem" 8 (2015) 217-244.

[24] N.E. Silina, A.G. Morozov, E.E. Gornostaeva, L.A. Smirnova, S.D. Zaytsev, Ultrasound-assisted synthesis of block copolymers of chitosan and D,L-lactide: structure and properties, Polym. Sci. Ser. B.59 (2017) 551-559.

[25] T. Abiraman, E. Ramanathan, G. Kavitha, R. Rengasamy, S. Balasubramanian, Synthesis of chitosan capped copper oxide nanoleaves using high intensity (30 kHz) ultrasound sonication and their application in antifouling coatings, Ultrason. Sonochem. 34 (2017) 781-791.

[26] A. Francesko, P. Petkova, E. Mendoza, T.Tzanov, Sonochemical synthesis and stabilization of concentrated antimicrobial silver-chitosan nanoparticle dispersions, J. Appl. Polym. Sci. 134 (2017) 1-8.

[27] S. Zahedi, J. S. Ghomi, H. Shahbazi-Alavi, Preparation of chitosan nanoparticles from shrimp shells and investigation of its catalytic effect in diastereoselective synthesis of dihydropyrroles, Ultrason. Sonochem. 40 (2018) 260-264.

[28] S. Khoee, A. Saadatinia, R. Bafkary, Ultrasound-assisted synthesis of pH-responsive nanovector based on PEG/chitosan coated magnetite nanoparticles for 5-FU delivery, Ultrason. Sonochem. 39 (2017) 144-152.

[29] E.P. Andrade, B.B.A. Costa, C.R. Chaves, A.M. de Paula, L.A. Cury, A. Malachias, G.A.M. Safar, STM-electroluminescence from clustered C_3N_4 nanodomains synthesized via green chemistry process, Ultrason. Sonochem. 40 (2018) 742-747.

[30] J. Jia, Y. Gai, W. Wang, Y. Zhao, Green synthesis of biocompatiable chitosan–graphene oxide hybrid nanosheet by ultrasonication method, Ultrason. Sonochem. 32 (2016) 300-306.

[31] Q. Wang, X. Yan, Y. Chang, L. Ren, J. Zhou, Fabrication and characterization of chitin nanofibers through esterification and ultrasound treatment, Carbohydr. Polym. 180 (2018) 81-87.

[32] G. Cravotto, P. Cintas, Molecular self-assembly and patterning induced by sound waves. The case of gelation, Chem. Soc. Rev., 38 (2009) 2684-2697.

[33] K. Isozaki, H. Takaya, T. Naota, Ultrasound-induced gelation of organic fluids with metalated peptides, Angew. Chem. Int. Ed., 46 (2007) 2855-2857.

[34] D. Bardelang, F. Camerel, J. C. Margeson, D. M. Leek, M. Schmutz, B. Zaman, K. Yu, D. V. Soldatov, R. Ziessel, C. I. Ratcliffe, J. A. Ripmeester, Unusual sculpting of dipeptide particles by ultrasound induces gelation, J. Am. Chem. Soc. 130 (2008) 3313-3315.

[35] S. Maity, P. Das, M. Reches, Inversion of supramolecular chirality by sonication-induced organogelation, Sci. Rep.-UK. 5 (2015) 16365.

[36] E. N. Fedoseeva, V. F. Uryash, N. Yu. Kokurina, and V. B. Fedoseev, Synthesis of chemical compounds of chitosan with betulin under nearly homogeneous conditions, Russ. J. Gen. Chem. 86 (2016) 2534-2540.

[37] A.P. Krasutsky, A. Pushechnikov, T. Sergeeva, PCT/US2006/011791 (2006) http:www.google.com/patents/WO 2006105354A1.

[38] P. Kovaricek, J.M. Lehn, Merging constitutional and motional covalent dynamics in reversible imine formation and exchange processes, J. Am. Chem. Soc. 134 (2012) 9446-9455.

[39] D. Sek, M. Grucela-Zajac, M. Krompiec, H. Janeczek, E. Schab-Balcerzak, E. New Glass Forming Triarylamine based Azomethines as a Hole Transport Materials: Thermal, Optical and Electrochemical Properties. Opt. Mat. 34 (2012) 1333-1346.

[40] L. Marin, A. van der Lee, S. Shova, A. Arvinte, M. Barboiu, Molecular amorphous glasses toward large azomethine crystals with aggregation-induced emission, New J. Chem. 39 (2015) 6404-6420.

[41] Y. Zhang, M. Barboiu, Constitutional Dynamic Materials-Toward Natural Selection of Function, Chem. Rev. 116 (2016) 809-834.

[42] S.M.L. Silva, C.R.C. Braga, M.V.L. Fook, C.M.O. Raposos, L.H. Carvalho, E.L. Canedo, Application of infrared spectroscopy to analysis of chitosan clay

nanocomposites infrared spectroscopy, in T. Theophile (Ed.), Materials Science, Engineering and Technology, In Tech, Europe, 2012, pp. 43-63.

[43] J. Kumirska, M. Czerwicka, Z. Kaczyński, A. Bychowska, K. Brzozowski, J. Thöming, P. Stepnowski, Application of spectroscopic methods for structural analysis of chitin and chitosan, Mar. Drugs 8 (2010) 1567-1636.

[44] A. Bonnet, J. Chisholm, W.D.S. Motherwell, W. Jones, Hydrogen bonding preference of equatorial versus axial hydroxyl groups in pyran and cyclohexane rings in organic crystals, Cryst. Eng. Comm. 7 (2005) 71-75.

[45] L. Marin, D. Ailincai, M. Mares, E. Paslaru, M. Cristea, V. Nica, B. C. Simionescu, Imino-chitosan biopolymeric films. Obtaining, self-assembling, surface and antimicrobial properties. Carbohydr. Polym., 117 (2015) 762-770.

[46] L. Marin, A. Bejan, D. Ailincai, D. Belei, Poly(azomethine-phenothiazine)s with efficient emission in solid state, Eur. Polym. J. 95 (2017) 127-137.

[47] A. Zabulica, E. Perju, M. Bruma, L. Marin, Novel luminescent liquid crystalline polyazomethines. Synthesis and study of thermotropic and photoluminescent properties, Liq. Cryst. 41 (2014) 252-262.

[48] M. Baron, Definitions of basic terms relating to low-molar-mass and polymer liquid crystals, Pure Appl. Chem. 73 (2001) 845-895.

[49] J.S. Chang, K.L.B. Chang, M.L.Tsai, Liquid-crystalline behavior of chitosan in malic acid, J. Appl. Polym. Sci. 105 (2007) 2670-2675.

[50] Y.-H. Cong, W.Wang, M. Tian, F.-B. Meng, B.-Y. Zhang, Liquid-crystalline behaviours of novel chitosan derivates containing singular and cholesteryl groups, Liq. Cryst. 36 (2009) 455-460.

[51] İ. Kaya, K. Temizkan, A. Aydın, Synthesis and characterization of aromatic and aliphatic ether bridged polymers containing carbazole moieties, Mat. Sci. Eng. B, 178 (2013) 863-874.

[52] D. Demus, L. Richter, Textures of liquid crystals, Verlag Chemie, Weinheim, 1978.

[53] L. Balau, G. Lisa, M.I. Popa, V. Tura, V. Melnig, Physico-chemical properties of chitosan films, Cent. Eur. J. Chem. 2 (2004) 638-647.

[54] I. M. El-Sherbiny, M. H. Yacoub, Hydrogel scaffolds for tissue engineering: progress and challenges, Global Cardiology Science and Practice 3 (2013) 316-342.

[55] Circular Dichroism: Principles and Applications. Second Edition Edited by Nina Berova (Columbia University), Koji Nakanishi (Columbia University), and Robert W. Woody (Colorado State University). Wiley-VCH: New York. 2000

[56] V.J. Tembu, M. K. Langat, N. R. Houch, D.A. Multholland, Use of circular dichroism to determine the absolute configuration of a pimarane diterpenoid from the southern african sclerocroton integerrimus (Euphorbiaceae), Nat. Prod. Commun. 9 (2014) 1131-1133.

[57] O. N. Malinkina, A. B. Shipovskaya , O. F. Kazmicheva, Optical rotatory dispersion and circular dichroism of the films based on chitosan in the form of polysalts and polybases, Proc of SPIE 9448 (2015), 944814-7.

[58] K. Ogawa, T. Yui, K. Okuyama, Three D structures of chitosan, Int. J. Biol. Macromol. 34 (2004) 1-8.

[59] L. A. Joyce, E. L. Regalado, C. J. Welch, Hydroxypyridyl imines: enhancing chromatographic separation and stereochemical analysis of chiral amines via circular dichroism, J. Org. Chem. 81 (2016) 8199-8205.

Abstract

The purpose of the study was to develop new antimicrobial hydrogels from natural resources that may promote wound healing and prevent bacterial skin infection. The new hydrogels were synthesized by crosslinking chitosan with a vanillin isomer, 5-methoxysalicylaldehyde, by a friendly and easy method. To characterize these hydrogels, their structural and morphological properties were explored by FTIR, ^{1}H-NMR, SEM, POM, and TGA. In view of the targeted application, swelling behavior, biodegradability, antimicrobial activity and biocompatibility were investigated *in vitro*. Structural and morphological studies confirmed the formation of new hydrogels *via* the imination reaction concomitant with the supramolecular organization. The hydrogels were highly porous with the average pore diameter around 80 µm, and a swelling rate controlled by the crosslinking density and medium pH. The hydrogels showed a progressive weight loss in the presence of lysozyme up to 35 %, during 21 days of testing. They proved non-cytotoxic effect on normal human dermal fibroblasts using MTS test and powerful antifungal activity against *Candida Albicans*, as determined by disk diffusion assay. All these properties indicate the new hydrogels as a promising option for the treatment of various skin lesions.

Keywords: chitosan, biodegradability, antifungal activity, non-toxicity

1. Introduction

In recent years, there was a growing global demand for new wound dressing materials to the increased resistance of pathogens to last-line antibiotics, which cause serious infections and wound-repair difficulties, leading to the loss of many human lives [1]. The ideal wound dressings should be easy and inexpensive to synthesize, sterile and non-toxic, biodegradable, to have good absorption of wound exudate and good gas permeability, and most importantly to have antimicrobial properties [2]. In this regard, varieties of wound dressing materials have been obtained either based on synthetic or natural polymers and are formulated in various forms such as membranes, films, fibers, topical formulations, transdermal patches, sponges, hydrogels and so on [3-6]. However, even some of these materials are effective in preventing bacterial infection of skin wounds, they suffer from several limitations such as high cost, weak mechanical performance, and difficulty to be removed without lesion damage, or inability to provide a moisture environment for acceleration of the wound healing process [7]. Considering these limitations, the development of more advanced wound dressings that are cost-effective is still a goal for researchers in clinical application [8].

Hydrogels are made up of a three-dimensional network that can absorb large amount of water and have a number of common physical properties with living tissues such as softness, elasticity and low interfacial tension, which are favorable for good compatibility and improve the healing process [9, 10]. Chitosan is known as the most important natural originating polymer that can be used to produce wound dressings due to its various versatile properties such as good biodegradability, biocompatibility, antibacterial and hemostatic effect, non-toxicity, bio-adhesivity and availability of functional groups for its modification [11-13]. In terms of wound treatment, chitosan-based hydrogels are considered as ideal materials which possess all the above properties [14, 15]. Compared to traditional wound dressings like cotton, wool or gauze, they are easier to peel off and degrade spontaneously, avoiding the discomfort and secondary trauma of dressing replacement [16]. Moreover, their porous structure and a suitable swelling ratio allow the oxygen permeation and exudate drainage while keeping a moist environment, which is beneficial for wound healing [17, 18] The main disadvantages of chitosan hydrogels for wound management are their drying up if they are not covered, difficulty to secure them, and poor mechanical stability in swollen state [19]. A promising approach to overcome these disadvantages can be the crosslinking of chitosan with natural monoaldehydes, which determine the enhancing of physical, chemical and mechanical properties (mechanical and thermal stability, swelling capacity, biodegradability and biocompatibility). Over last years, our group demonstrated that chitosan crosslinking with monoadehydes, *via* formation of imine units

and their self-assembling into clusters, is a simple method towards hydrogels with properties tailored by a proper choice of the aldehyde [20-27].

Taking into account these data, this paper reports the synthesis of chitosan hydrogels with inherent antimicrobial properties by crosslinking with a natural monoaldehyde, 5-methoxysalicylaldehyde (A). It should be highlighted that this aldehyde is one of the isomers of vanillin, a naturally occurring derivate of benzaldehyde, which has already demonstrated significance in food, cosmetics, chemical and pharmaceutical industries [28]. Its choice was done targeting biocompatible hydrogels with antimicrobial properties capable to promote wound healing and prevent the bacterial skin infections. Moreover, compared to traditional wound dressings, these hydrogels are expected to be biodegradable, avoiding by this the traumatic debridement. The hydrogels were characterized in relationship with the envisaged applications, their properties such as swelling in media with different pH, biodegradation, biocompatibility, self-healing and antimicrobial activity being investigated. They showed porous morphology and good swelling ability which can assure the exudate drainage maintaining a moist environment useful to promote wound healing. They were thermally stable, biodegradable and pH-sensitive, and presented antimicrobial performance against *Candida albicans*, self-healing behavior and good biocompatibility, indicating great potential for use in the treatment of skin lesions. To the best of our knowledge, this is the first study which reports the synthesis and performances of chitosan hydrogels cross-linked with the natural monoaldehyde, 5-methoxysalicylaldehyde.

3.1.2. Material and methods

2.1. Materials

Low molecular weight chitosan, 5-methoxysalicylaldehyde of 98% purity, (**A**), ethanol (99.8%) and glacial acetic acid (99%) were purchased from Aldrich Co. (USA) and used as received. The average viscometric molecular weight of chitosan (M_v) was calculated by viscosimetry (M_v=198kDa) and the deacetylation degree (DA=82%) was calculated by ^{1}H-NMR (Fig. S1 and Fig. S2) [13]. The total of the free amino groups of chitosan was calculated considering the DA. Acetate buffer solution of pH=5.5 and phosphate buffer (PBS) of pH=7.4 and 8.5 were prepared in our laboratory, as already reported [20-23]. Bidistilled and ultrapure water were obtained in our laboratory, too.

2.2. Synthesis of 5-methoxysalicyl-imine-chitosan hydrogels (Hx)

The synthesis was carried out by acid condensation reaction of chitosan with 5-methoxysalicylaldehyde (**A**), adapting a procedure reported for other chitosan/aldehyde

systems [20]. 0.480 g chitosan (corresponding to $2.32*10^{-3}$ mmol glucosamine repeating units) were dissolved in 24 mL acidic water (0.7% acetic acid solution: 168 μL of acetic acid in 24 mL of water) under vigorous magnetic stirring (750 rpm). Further, the chitosan solution was heated at 55°C, and a 2% solution of 5-methoxysalicylaldehyde (**A**) in ethanol was slowly dropped into it and the reaction mixture was maintained until hydrogelation occurred. In order to reach hydrogels with different crosslinking degrees, the 5-methoxysalicylaldehyde (**A**) amount was varied to attain molar ratios of the NH_2 and CHO functional groups from 1/1 up to 6/1 (Table 1). The hydrogelation time depended on the NH_2/CHO molar ratio, varying from 1 minute to 7 days as the aldehyde amount decreased (Table 1). In order to remove the ethanol, the vials were kept uncovered up to the initial volume of chitosan solution was reached. The as obtained hydrogels (noted ***Hx***, where **x** is the molar ratio of the NH_2/CHO functional groups) appeared as transparent, deep yellow semisolid materials, with smooth texture (Scheme 1). Their corresponding solid materials (xerogels) were prepared by hydrogels' lyophilization. The xerogels weight was similar with that of the initial reagents, indicating no mass loss during lyophilization, and implicit the total reaction of the reagents.

Tabel 1. The reaction parameters and codes of the studied hydrogels (***Hx***)

Code	**H1**	**H1.5**	**H2**	**H3**	**H4**	**H5**	**H6**
NH_2/CH=O	1/1	1.5/1	2/1	3/1	4/1	5/1	6/1
Chitosan (mg/mmol)	480/$2.32*10^{-3}$						
A (mg/mmol)	353/ $2.32x10^{-3}$	235/ $1.54x10^{-3}$	177/ $1.16x10^{-3}$	117 $7.7x10^{-4}$	88/ $5.8x10^{-4}$	71/ $4.61x10^{-4}$	59/ $3.9x10^{-4}$
Water (mL)	24						
Ethanol (mL)	17.66	11.77	8.83	5.88	4.42	3.53	2.94
Acetic acid (ml)	0.168						
Gelation time	1min	2 min	5 min	30 min	1day	2days	7days
Xerogel (g)	0.833	0.715	0.657	0.597	0.568	0.551	0.539

A: 5-methoxysalicylaldehyde;

2.3. Characterization

2.3.1. The dry state of the hydrogels (xerogels) was obtained by freezing in liquid nitrogen and further lyophilisation using Labconco Free Zone Freeze Dry System equipment, at -52 °C and 1.510 mbar for 48 hours.

2.3.2. ***The ^{1}H-NMR spectra* (*NMR*)** were achieved on a Bruker Advance DRX 400 MHz Spectrometer equipped with a 5 mm QNP direct detection probe and z-gradients. For NMR measurements, the hydrogels were prepared directly into NMR tubes using deuterated water. The chemical shifts were reported as δ values (ppm) relative to the residual peak of deuterated water.

2.3.3. Fourier transformed infrared spectroscopy (FTIR). ATR-FTIR spectra were registered with a Bruker Vertex 70 Ettlingen FTIR spectrometer, on pellets obtained by pressing 20 mg of xerogels into a hydraulic press at 2 N/m^2. The spectra were recorded in the 600–4000 cm^{-1} spectral range, with 32 scans at 4 cm^{-1} resolution. The presence of the imine linkage was confirmed by deconvolution of the 1690-1615 cm^{-1} region of the FTIR spectra. The overlapped peak positions from this region were determined with the second derivative. After that, the stretching vibration regions were deconvoluted by a curve-fitting mode, and the areas were calculated with a 50% Lorentzian and 50% Gaussian function. The OPUS 6.5 software and OriginProBit9 were used to perform the curve-fitting analysis [29].

2.3.4. To gain an insight on the hydrogel morphology, images of the corresponding xerogels were acquired with a field emission ***Scanning Electron Microscope (SEM)*** EDAX – Quanta 200 at accelerated electron energy of 20KeV.

2.3.5. ***Polarized light microscopy*** observations were performed with a Zeiss Axio Imager.A2m, camera Axiocam 208cc, Carl Zeiss AG, (Oberkochen, Germany) microscope, on thin slices of hydrogels.

2.3.6. ***X-ray diffraction investigation*** was done on a Rigaku Miniflex 600 diffractometer by CuKα-emission in the angular range 2–40º (2θ) using a scanning step of 0.0025º and a recording rate of 1º/min.

2.3.7. The ***thermogravimetric analysis (TGA)*** was performed on xerogel samples with a Discovery TGA 5500 equipment, under nitrogen atmosphere, at the constant heating rate of 10°C/min from 30 to 600ºC. The amount of each sample was approx. 7 mg. The temperature corresponding to 10% (T_{10}) weight loss, and the temperature of maximum decomposition rate, corresponding to the peak in DTG curve (T_{dec}), have been taken as characteristic conditions when discussing the thermal stability.

2.3.8. The UV-Vis spectra were recorded on an ***UV-visible spectrophotometer*** (Perkin Elmer, Lambda 10). The *in vitro* aldehyde release was investigated by monitoring the released aldehyde by quantitative absorption spectroscopy, as follows. 120 mg hydrogel was immersed into a vial containing 10 mL of ultrapure water, at 37ºC. At fixed intervals, 2 mL aliquots were withdrawn and replaced with 2 mL fresh ultrapure water. The supernatant samples were

collected and subjected to aldehyde absorbance measurements by UV-vis spectroscopy, recording the specific absorption band at 258.87 nm. Further, the absorbance values were fitted on a predetermined calibration curve to give the aldehyde concentrations. The cumulative release of **A** was calculated with the equation: % **A** = $[(10C_n + 2\Sigma C_{n-1})/m_o]$ x 100, and was plotted versus time to give the release kinetic, where C_n and C_{n-1} represent the concentrations of the aldehyde in the supernatant after n and n-1 withdrawing steps, respectively, and m_o, correspond to the aldehyde's content.

2.3.9. ***Swelling behavior and stability of the hydrogels in media with different pH***

The swelling ability of the hydrogels was investigated on the samples which showed the most important properties (***H1.5***, ***H2*** and ***H3***) in distilled water and buffer solution of different pH = 5.5, 7.4 and 8.5, at 37°C [4]. Certain amounts around 100 mg of hydrogels were immersed into vials containing 10 mL of swelling media, and the samples were taken off and weighted at known time periods until they reached a constant mass. After that, they were washed with ultrapure water and dried by lyophilisation to calculate their weight loss. The percentage of swelling ratio (SR) of the hydrogels was calculated using the equation (1):

$$SR = (W_s - W_d)/W_d \times 100 \quad \textbf{(1)}$$

where W_s and W_d are the weights of the swollen and the initial hydrogels, respectively. The weight loss percent was calculated with equation (2):

$$\text{Weight loss } \% = W_0 - W_t/W_0 \times 100 \quad \textbf{(2)}$$

where W_0 is the initial weight of the freeze-dried hydrogels; W_t is the weight of the freeze-dried hydrogel at the end of swelling experiment (2 days). To know exactly the initial weight of the freeze-dried hydrogels, the same amount of the hydrogels used in the swelling study was lyophilized during 24h.

The hydrolytic stability of the hydrogels was visually monitored by immersing pieces of hydrogels of 100 mg in the same media used in the swelling study, over 2 days and 3 months [30-32].

2.3.10. In vitro enzymatic biodegradation of the hydrogels

The hydrogels were incubated in solution of lysozyme in PBS (pH=8.5), 10mg/L (400000U/L) at 37 °C for 21 days. The incubation medium was refreshed at every three days in order to maintain the enzymatic activity. The samples were carefully taken out at predetermined time intervals of 1, 2, 3, 4, 7, 14 and 21 days, washed with ultrapure water, and lyophilized [33]. The hydrogels' biodegradation was assessed by calculating the mass loss using the equation (3):

$$\text{Weight loss} = (W_0 - W_t)/W_0 \times 100$$

(3)

where W_0 is the initial weight of the freeze-dried hydrogels and W_t is the weight of the freeze-dried hydrogel at the time t.

2.3.11. ***Cytotoxicity of chitosan hydrogels***

Cell culture: Normal human dermal fibroblasts (NHDF, PromoCell, Heidelberg, Germany) were grown in alpha-MEM medium (Lonza, Basel, Switzerland) supplemented with 10% fetal bovine serum (FBS, Gibco, Thermo Fisher Scientific, Waltham, MA USA) and 1% Penicillin-Streptomycin-Amphotericin B mixture (Lonza, Basel, Switzerland) in humidified atmosphere with 5% CO_2, at 37 °C.

Cytotoxicity of chitosan hydrogels: Cytotoxicity of ***Hx*** hydrogels was assessed by MTS assay using the CellTiter 96® AQueous One Solution Cell Proliferation Assay (Promega, Madison, WI USA), according to the manufacturer instructions and direct contact procedure adapted from ISO 10993-5:2009(E) [34]. For this purpose, cells were seeded at a density of 5×10^3 cells/mL into 96-well tissue culture-treated plates in 100 µL culture medium/well and allowed to adhere for 24h. Cells were then incubated for another 24 hours with 200 µl culture medium and 10 (± 0.01) mg of each hydrogel sample (3mm diameter). Before incubating, the hydrogel samples were immersed in 70% ethanol, washed with ultrapure water, with culture medium and exposed to UV light (253.7 nm) for 30 minutes. Control cells were incubated only with culture medium. The next day, the medium in the wells containing the tested material was replaced with 100 µl fresh medium and MTS reagent (20 µL) was added 1-3 hours prior to absorbance readings at 490 nm on a FLUOstar® Omega microplate reader (BMG LABTECH, Ortenberg, Germany). Experiments were done in triplicate and treated cell viability was expressed as percentage of control cells' viability. Graphical data were expressed as means ± standard error of the mean. Statistical analysis was performed using GraphPad Prism 7 with One-way Anova using Kruskal-Wallis test with Dunn's multiple comparisons test. The differences were considered statistically different when $p<0.05$.

Cell morphology: To confirm the MTS assay, morphology of the cells exposed to the chitosan hydrogel samples was analyzed by optical microscopy. The hydrogel samples were cut into 1 cm diameter pieces, immersed in 70% ethanol, washed with ultrapure water, with culture medium and sterilized by exposure to UV light (253.7 nm) for 30 minutes. The samples were placed into a 24-well tissue culture treated plate and NHDF cells were seeded onto sterilized hydrogels at a density of $1x10^5$ cells/mL in 1 mL culture medium/well. Cells were then incubated for 24 hours. Control cells were incubated only with culture medium. After 24

hours, brightfield images were acquired with a Leica DMI 3000B inverted microscope (Wetzlar, Germany).

2.3.12. *Antimicrobial activity*

The antimicrobial activity screening of the hydrogels was determined by disk diffusion assay [35] against three bacterial strains: *Staphylococcus aureus* ATCC25923, *Escherichia coli* ATCC25922 and *Enterococcus faecalis* ATCC 29212, two yeast strains *Candida albicans* ATCC10231 and *Candida glabrata* ATCC 2001, and three fungal strains: *Penicillium chrysogenum* ATCC10106, *Cladosporium cladosporioides* ATCC16022 and *Aspergillus brasiliensis* ATCC9642. All microorganisms were stored at -80 °C in 20-40% glycerol. The bacterial strains were refreshed on tryptic soy agar (TSA) at 37 °C for 24 hours. The yeast strains were refreshed on Sabouraud dextrose agar (SDA) and the fungal strains were refreshed on potato dextrose agar (PDA) for *C. cladosporioides* and *A.brasiliensis* and malt extract agar (MEA) for *P. chrysogenum* at 25°C for 72 hours. Microbial suspensions were prepared with these cultures in sterile solution to obtain turbidity optically comparable to that of 0.5 McFarland standards. Volumes of 0.2 ml from each inoculum were spread on the Petri dishes. The sterilized paper disks were placed on the plates and an aliquot (50 µl) of the samples was added. To evaluate the antimicrobial properties, the growth inhibition was measured under standard conditions after 24 of incubation at 37°C for the bacterial strains and the yeast strains and after 72 hours at 25ºC for the fungal strains. All tests were carried out in triplicate to verify the results. After incubation, the diameters of inhibition zones were measured by using Image J software and were expressed as the mean ± standard deviation (SD). Statistical analysis was performed XLSTAT software [36].

Statistics

All experiments were done in triplicate and the data were considered as the mean ± standard deviation (SD).

3. RESULTS AND DISCUSSION

A series of six hydrogels was prepared by acid condensation reaction of chitosan with 5-methoxysalicylaldehyde (***A***), varying the molar ratio between glucosamine units of chitosan and aldehyde groups (Table 1). The schematic representation of their synthesis was shown in Scheme 1. As previously demonstrated for crosslinking of chitosan with monoaldehydes, the hydrogelation was expected to take place due to the formation of imine linkages on the chitosan chains, and the self-ordering of these new formed imine units into clusters, playing the role of crosslinking nodes for chitosan chains [20-27]. This hydrogelation pattern was confirmed by

structural and supramolecular investigations by ^{1}H-NMR, FTIR, WRXD, and POM, which were performed on the hydrogels and their corresponding xerogels and analyzed in details.

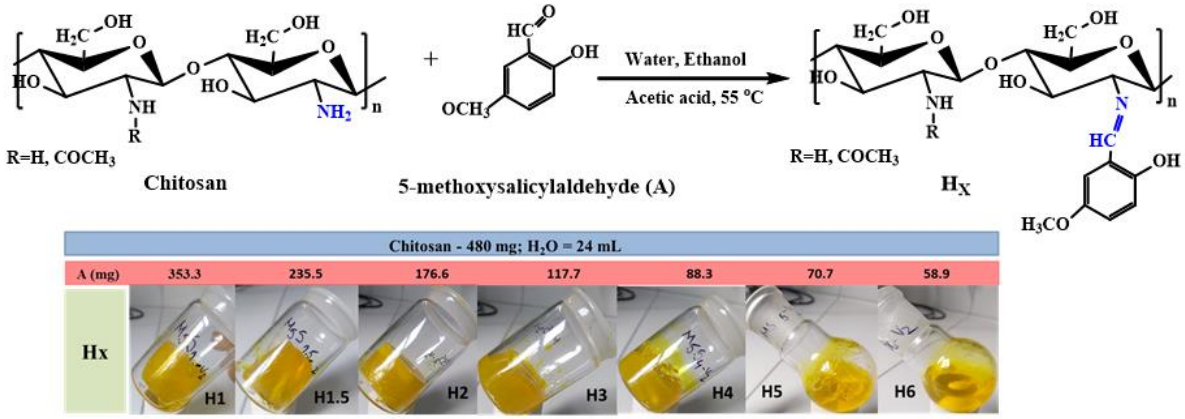

Scheme 1. Schematic representation for the hydrogels' obtaining (***Hx)***

3.1. Structural characterization

The ***^{1}H-NMR spectra*** of hydrogels (***H1.5-H5*)** revealed the formation of imine linkage by the occurrence of the chemical shift of imine proton as a single band at 8.39 ppm [20]. During the first 3 hours after hydrogelation, the aldehyde proton was also seen at 9.82 ppm, but it almost completely disappeared after 7 days, indicating the progressive conversion of aldehyde into imine units (Fig.1, Fig. S3). Compared to other hydrogels prepared from chitosan and monoaldehydes [21, 23, 24, 33] the high imination yield was attributed to the stabilization of the imine linkages by an intramolecular H-bond with the neighbor proton from hydroxyl group, by a "clip-effect" [22, 37, 38]. The chemical shifts of the other protons from 5-methoxysalicylaldehyde and chitosan were also present in the spectra.

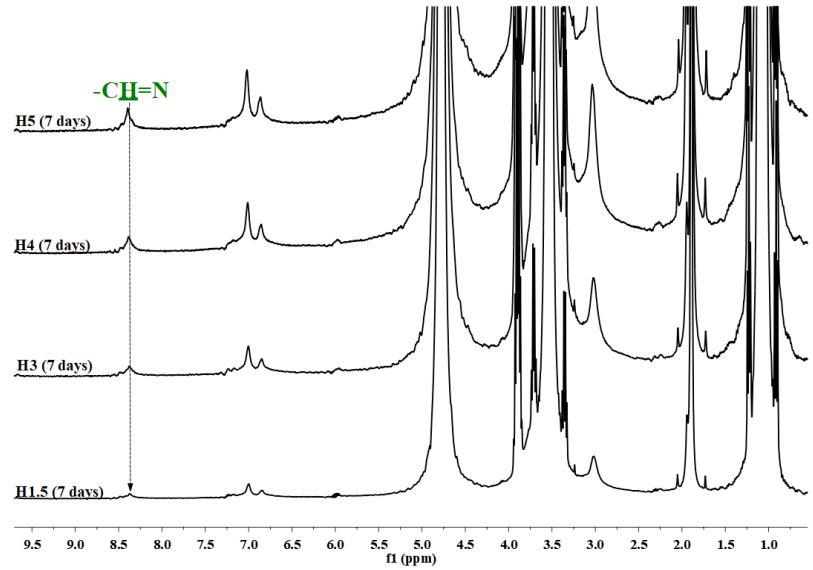

a)

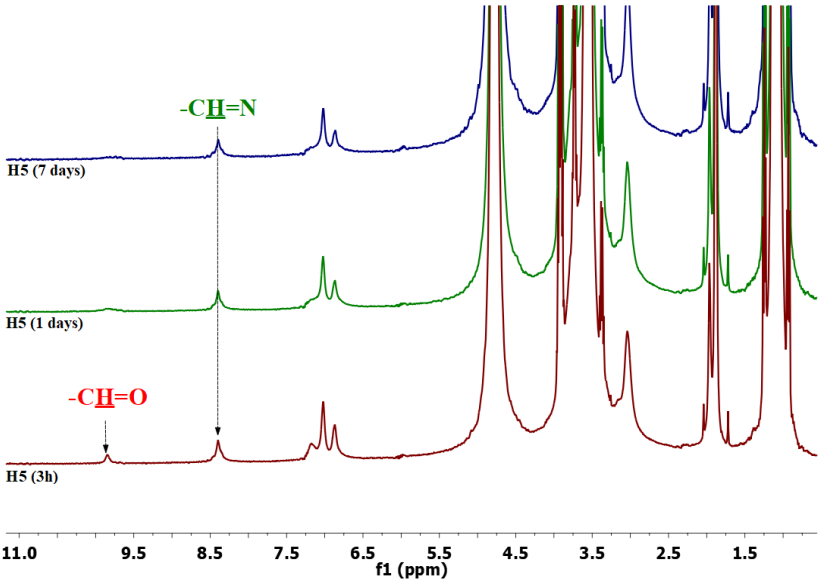

b)

Fig. *1*. (a) NMR spectra of representative hydrogels recorded after 7 days since hydrogelation; (b) NMR spectra of the sample ***H_5*** recorded at different moments over 7 days

FTIR spectra of the corresponding xerogels showed modifications compared to those of precursors, i.e. chitosan and 5-methoxysalicylaldehyde, consistent with the formation of the imine linkages (Fig.2, Fig.S4). Thus, the broad band characteristic for the vibration of amide group in chitosan (around 1639 cm^{-1}) transformed into a sharp band with maximum at 1637 cm^{-1} with a shoulder to higher wavenumbers, the most probably resulting from the overlapping of imine and amide bands (Fig. 2a). The deconvolution of 1690-1615 cm^{-1} spectral domain, indeed revealed the appearance of a new band at 1633 cm^{-1}, characteristic for the vibration of imine

linkage stabilized by a “clip-effect” (Fig. 2b, 2c) [20]. No characteristic band for the vibration of aldehyde group of 5-methoxysalicylaldehyde (1661 cm^{-1}) was detected confirming its total consumption. Comparing the xerogels’ spectra, a diminishing of the intensity of the imine absorption band was evident along the decreasing the ***A*** reagent (Fig.S4) [39]. Other absorption bands characteristic to the aliphatic stretching vibration originating from chitosan (2924 and 2876 cm^{-1}) and the double bond stretching vibrations originating from 5-methoxysalicylaldehyde (1591 and 1486 cm^{-1}) were also present [26]. Spectral modifications were also observed in the domain characteristic for the vibrations of amine and hydroxyl groups in chitosan and their *intra*- and *inter*- molecular H-bonds. While chitosan showed a broad band with two maxima at 3401 and 3283 cm^{-1}, attributed to the symmetric and asymmetric vibration of the amine units, the xerogels showed a maximum around 3459 cm^{-1}, possible correlated with the new intra-molecular H-bonds between imine nitrogen and H atom of the hydroxyl groups [20, 40].

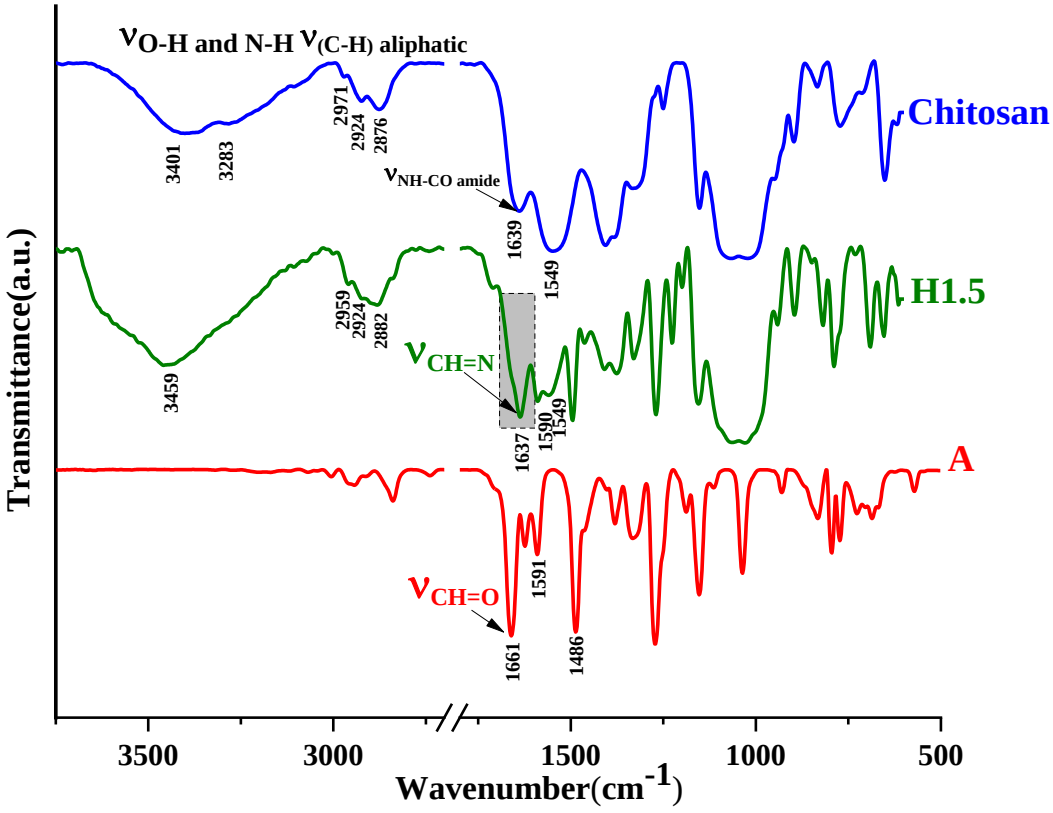

a)

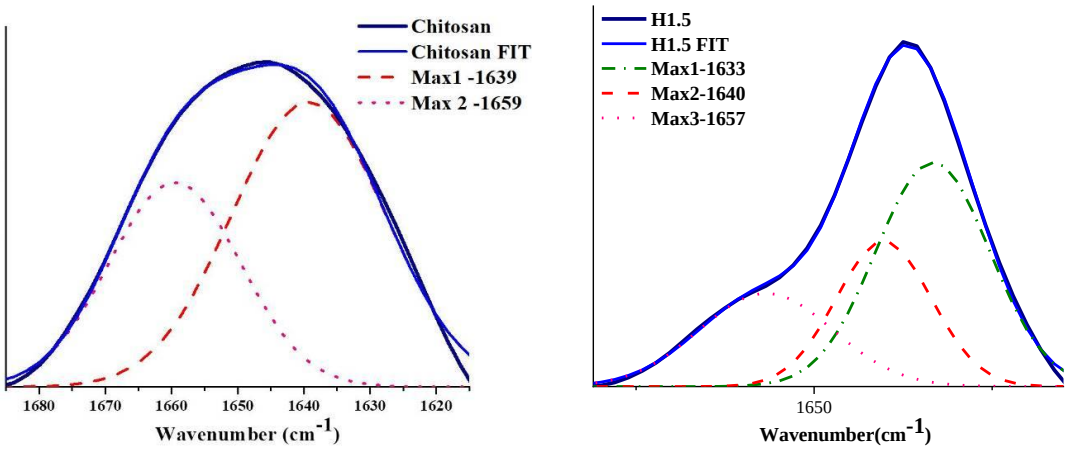

b) **c)**

Fig.2. a) The FTIR spectra of the ***A***, ***H1.5*** and ***chitosan*** and *b)* deconvolution of the 1690-1615 cm^{-1} spectral domain for chitosan and ***H1.5***.

3.2 Supramolecular characterization

The preliminary investigation of the supramolecular ordering of the imine units into clusters was done by observing the hydrogels under polarized light. As can be seen in Fig.3a,b, the hydrogels showed strong birefringence with a banded texture, characteristic for layered architectures of the ordered clusters [20, 22]. The hypothesis of the ordered clusters was also supported by the yellowish luminescence of the hydrogels when illuminated with an UV-lamp, attributable to the emission of new fluorophores formed *via* the space conjugation of the imine subfluorophores (Fig.3c, d) [41].

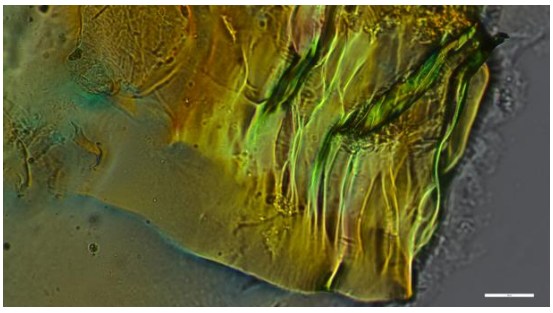

a) H1

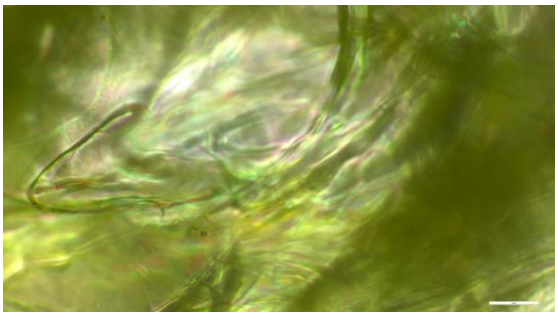

b) H4

c) H1

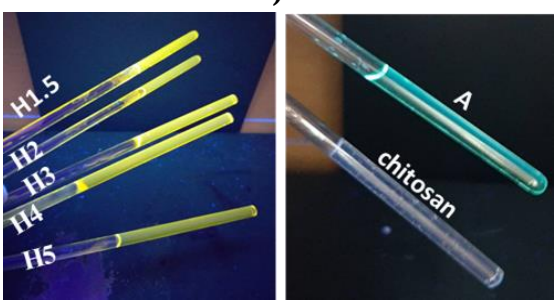

d) H1.5-H5, A and Chitosan

Fig. 3. a,b) POM images of representative hydrogels (scale: 50 μm) and c,d) hydrogels and chitosan and **A** solutions illuminated with an UV lamp

Further, in order to evidence the self-assembling of the newly formed imine units, wide angle X-ray diffraction on xerogels was performed. As can be seen in Fig. 4 the chitosan diffractogram suffered major modification after hydrogelation with 5-methoxysalicylaldehyde, mainly consisting in the occurrence of a sharp reflection band at 5.9 º, characteristic to a layer periodicity [20-24]. The corresponding inter-layer distance of 14.99-14.04 Å was in good agreement with the inter-layer spacing into a layered architecture with partial overlapping of the imine units of adjacent layers [42]. Besides, the broad reflection of chitosan at 21.8 º shifted to lower angle at 20.7º and a new reflection appeared at 13º, consistent with inter-chain (4.4 Å) and inter-molecular (6.8 Å) distances into the 3D ordered clusters (Table S1) [20-24]. Regarding the WXRD diffractograms of different xerogels, it can be observed that the intensity of the inter-layer reflection decreased along the imination degree, in agreement with the decreasing of the clusters' density (Table S1).

All these data confirmed that the formation of the imine units and their self-ordering into clusters are the driving forces of the hydrogelation process of chitosan with 5-methoxysalicylaldehyde.

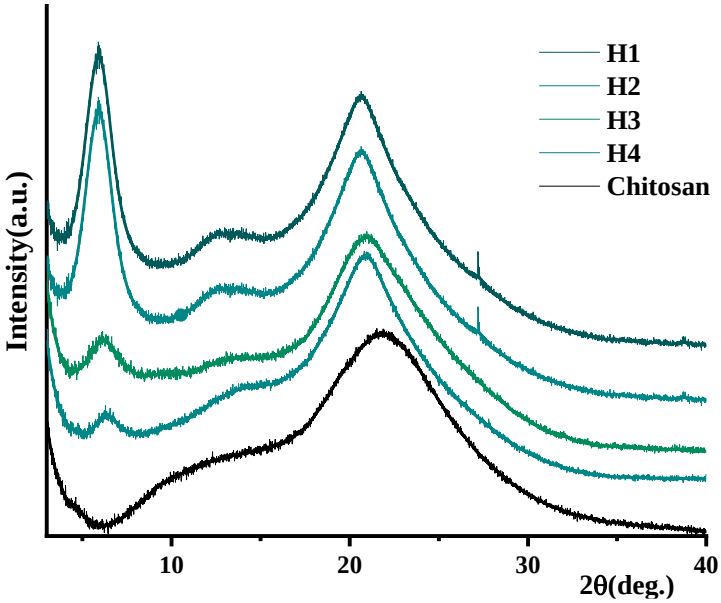

Fig. 4. WXRD of the chitosan and representative xerogels

3.3. Thermogravimetric Analysis (TGA)

Thermal analysis of the xerogels and their precursors revealed interesting aspects related to the physicochemical properties of the hydrogels. First, the rapid mass loss characteristic to

the aldehyde volatilization [43] was not detected in the ATG/DTG curves of the xerogels (Fig.5a,b), confirming its chemical bonding to chitosan chains by imination, as ^{1}H-NMR and FTIR spectra indicated. TGA curves showed an evident improvement of the thermal stability as the imination degree increased, i.e. the T_{10} (corresponding to 10% weight loss) recorded at 110^{o}C for chitosan, progressively shifted from 112^{o}C (***H5***) to 273^{o}C (***H1***) for xerogels. The improving of thermal stability was attributed to the effect of crosslinking by imination and formation of ordered clusters. The ***H1*** showed the highest thermal stability, according to a dense network determined by the almost total imination of the amine groups of chitosan. A deeper insight gained from the DTG curves (Fig. 5b) show that the first degradation stage corresponding to the evaporation of adsorbed water occurred at lower temperatures for xerogels compared to pristine chitosan, in agreement with the imination occurrence which disturbed the H-bonds of water to amine units [44]. The most important thermogravimetric characteristics of the representative xerogels, obtained from the thermograms are listed in Table S2.

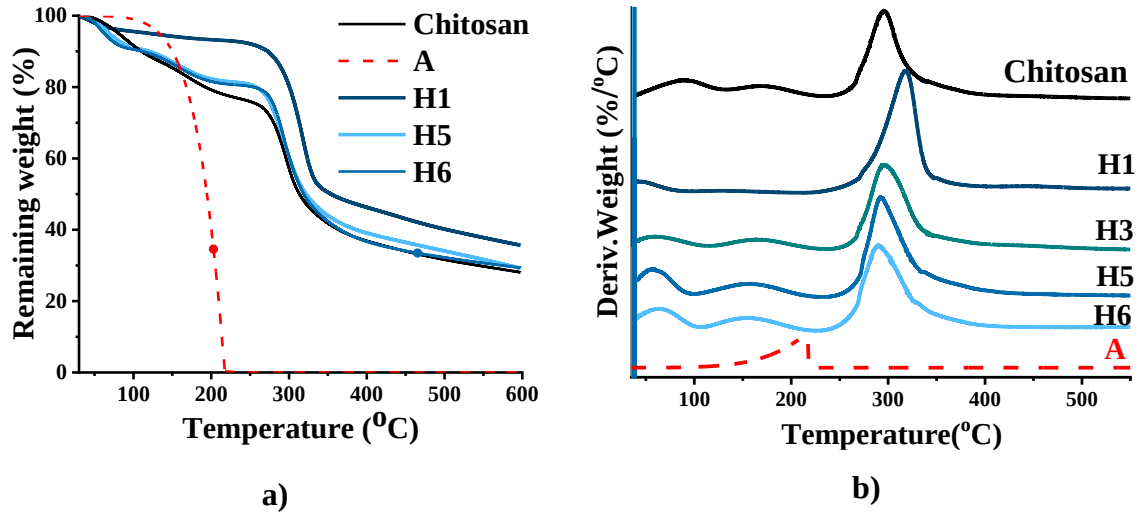

***Fig. 5. a*)** The thermograms and **b**) DTG curves of chitosan, **A** and some representative freeze-dried hydrogels

3.4. Morphology of the 5-methoxysalicyl-imine-chitosan hydrogels

SEM images acquired on freeze-dried hydrogels clearly showed the presence of large quantities of interconnected pores with irregular shape indicating a porous or fibrous structure, depending on the aldehyde content [45]. As can be seen in Figure 6 and Figure S5, the hydrogel with lowest crosslinking degree (***H6***) presented a fibers network, those with intermediate crosslinking degree displayed irregular pores and fibers connected together (***H3***, ***H4*** and ***H5***), and those with higher crosslinking degree (***H1, H1.5*** and ***H2***) showed interconnected pores

with diameters around 85-100 μm. It appears that the hydrogel morphology can be tuned by a proper choice of the amount aldehyde crosslinker.

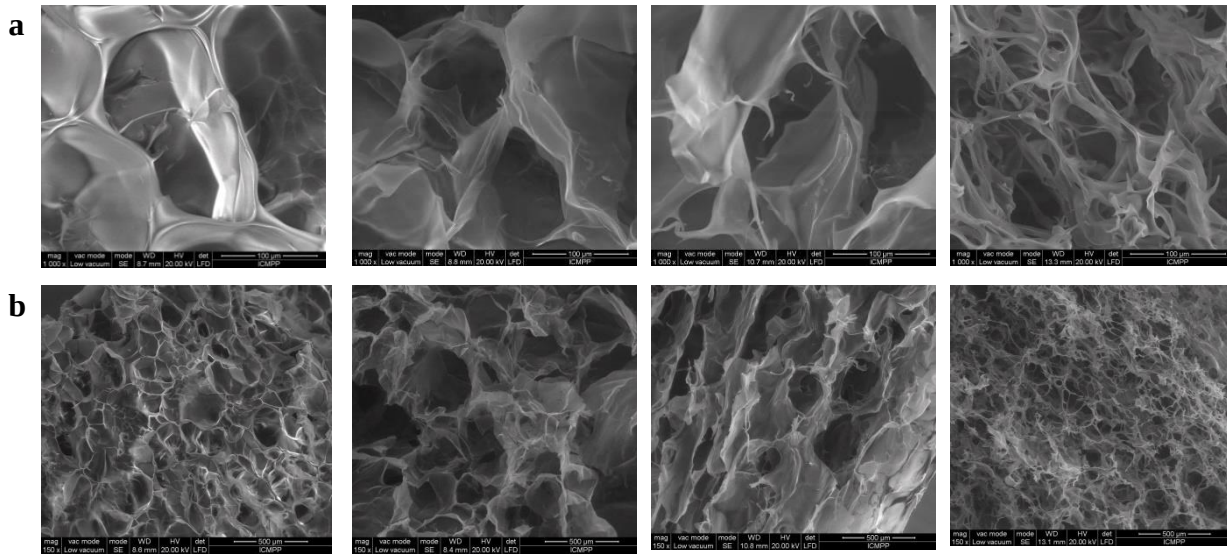

Fig.6. SEM images of freeze-dried hydrogels at different magnifications: a) 1000x; b) 150x

3.5. Cytotoxicity of chitosan hydrogels (MTS assay)

The main condition for *in vivo* application of materials is their biocompatibility. The studied hydrogels were obtained from natural originating reagents, which should account for non-toxicity, biodegradation and biocompatibility, assuring a good acceptance into tissues [46]. In this view, the response of NHDF cells at the contact with the studied hydrogels and pristine reagents was investigated, according to ISO 10993-5:2009(E) test for medical devices that recommend the use of materials for biomedical purposes for cell viability higher than 70% [34]. As can be seen in figure 7, the ***H1.5***, ***H2*** and ***H3*** proved suitable biocompatibility for *in vivo* applications, while those with higher or lower crosslinking degrees showed higher cytotoxicity than accepted for medical devices.

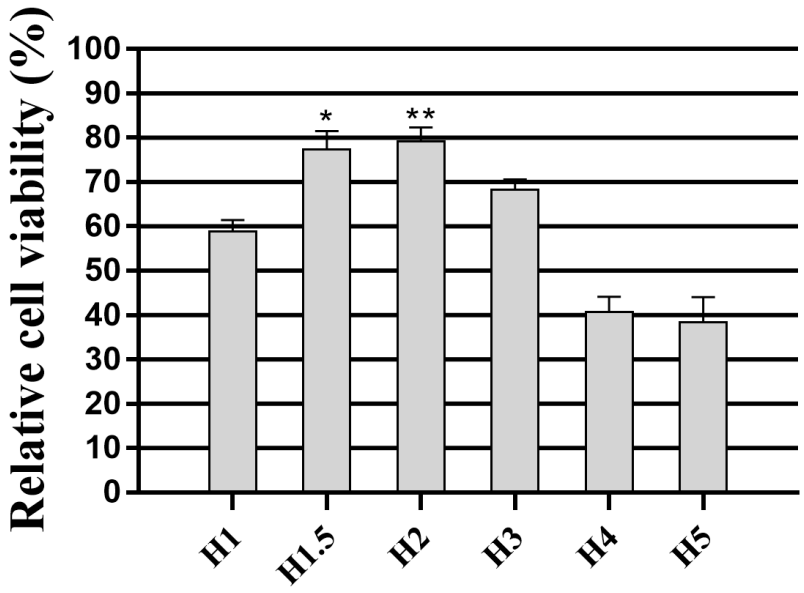

Fig.7. Cell viability of normal human dermal fibroblasts (NHDF) after 24 hours exposure to hydrogels, compared to untreated cells. The results are presented as mean value ± the standard error of the mean (SEM), n = 5; * $p<0.05$ (H1.5 vs. H4, H1.5 vs. H5) and ** $p<0.01$ (H2 vs. H4, H2 vs. H5).

Cell Morphology

Brightfield images were acquired only for those samples that indicated higher viability. The morphology of cells incubated with ***H1.5*** and ***H2*** was normal, NHDF cells keeping their characteristic elongated form (Figure 8). Some of the cells incubated with ***H3*** have a rounded shape, which indicates their partial detachment from the substrate, this being in agreement with the result of the MTS test. Finally, the increased viability of cells incubated in the presence of hydrogels indicates their usefulness in wound healing applications.

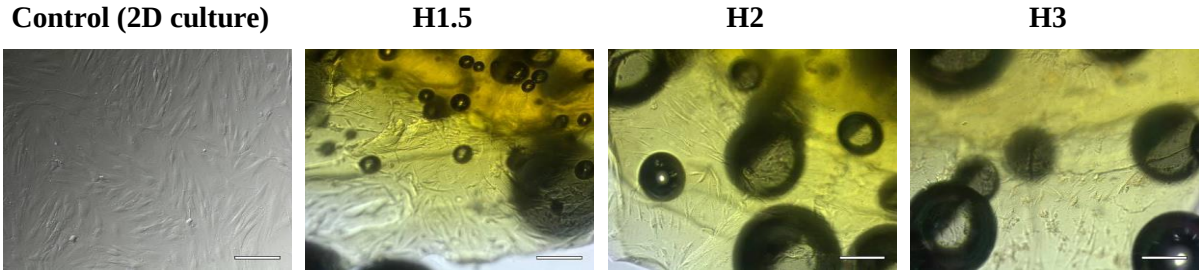

Fig.8. Brightfield images indicating cell morphology in control and in culture-treated plates. The scale represents 200 μm (bubbles in the treated plates are bubbles air in hydrogels).

3.6. Antimicrobial activity

The choice of 5-methoxysalicylaldehyde **(A)** as aldehyde for chitosan's hydrogelation took into consideration its natural origin which increases the probability of *in vivo* biocompatibility and also its potential antimicrobial activity demonstrated against some pathogens such as *Aspergillus flavus* [47,48] *Aspergillus fumigatus*, *A. terreus* and *Penicillium expansum* [49], *Mycobacterium avium* [50] and *Escherichia coli* [51].

In this regard, the antimicrobial activity of the hydrogels was investigated on relevant pathogens that play essential role in human health, such as gram positive (*S.aureus*), gram-negative (*E.coli*), yeast (*C. albicans* and *C. glabrata*) and fungal (*P. chrysogenum*, *C. cladosporioides*, *A. brasiliensis*) strains by agar disk diffusion method. For a proper comparison, chitosan and aldehyde precursors were investigated as controlso, at the same concentration as in hydrogels. The results were presented in Fig. 9 and Table S3.

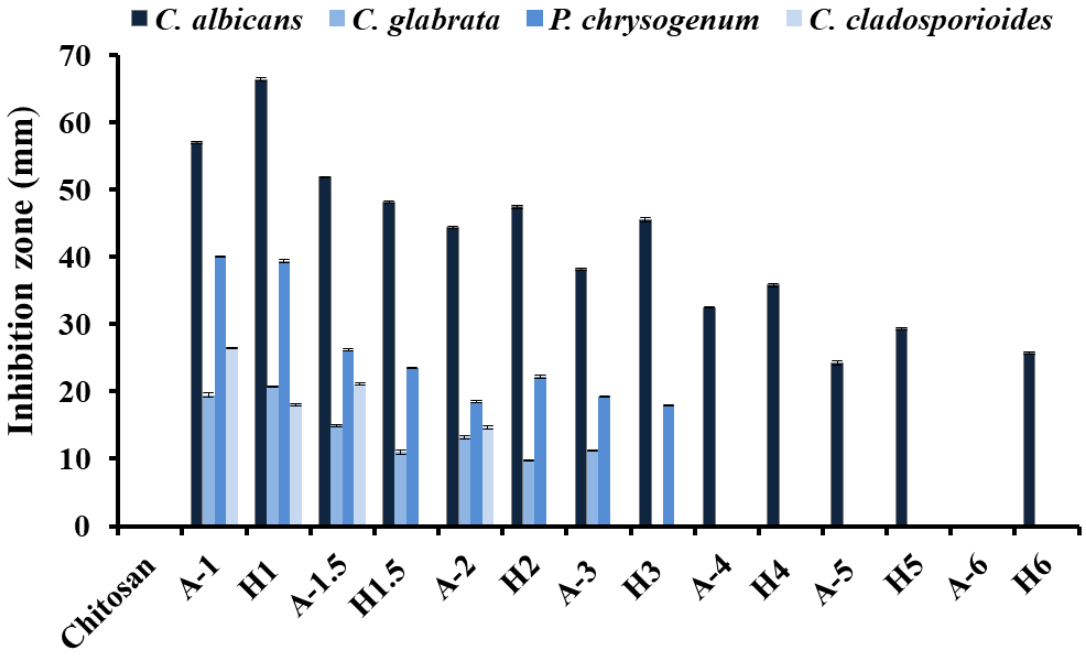

a)

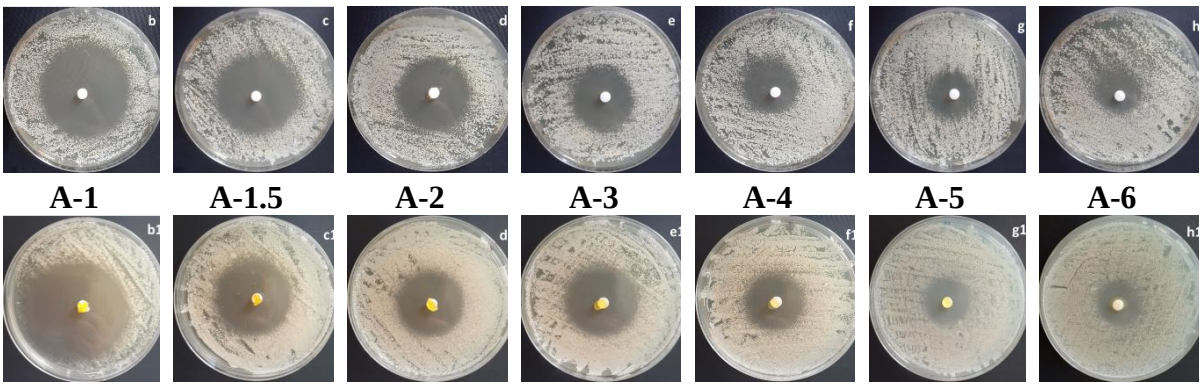

b)

Fig. 9. a) Graphical representation of the inhibition zones on various fungal strains and b) representative images for the case of *C.albicans*

Contrary to the literature data, chitosan did not present any antimicrobial activity (see Table S3 and Fig. S5) [52-54]. The hydrogels and 5-methoxysalicylaldehyde (**A**) presented concentration dependent antifungal activity, the inhibition zone decreasing once the 5-methoxysalicylaldehyde concentration decreased (Fig. 9, Table S3). The highest activity was noticed against the *C. albicans*, reaching an inhibition zone of 66 mm in the case of hydrogel ***H1*** (Fig. 9). Interesting enough, the hydrogels were slightly more efficient against *C. albicans* compared with their aldehyde controls. High antifungal activity was also displayed against *P. chrysogenum* (around 40 mm), and good activity was recorded against *C. glabrata* (around 20 mm) and *C. cladosporioides* (around 20 mm), for the highest concentrations of the aldehyde and the corresponding hydrogels. In these cases, the antifungal activity of hydrogels did not exceed that of the aldehyde control, on contrary it was slightly lower. No inhibition zone was recorded against *S. aureus*, *E. coli* and *E. faecalis* for the hydrogels or corresponding aldehyde controls. From these data it appeared that the studied hydrogels have a specific affinity for *C. albicans* yeast, higher than their precursors. This is an intriguing finding, considering the aldehyde mobility in the two samples: (i) high mobility in solution assuring a very fast diffusion of the 5-methoxysalicylaldehyde molecules into the yeast medium, and (ii) low mobility in hydrogel state with 5-methoxysalicylaldehyde covalently bonded *via* imine linkage to the chitosan. It is possible as the reversible nature of imine linkage to play an important role in this behavior. It is expected that the reaction equilibrium to be shifted to the reagents once 5-methoxysalicylaldehyde is consumed in the process of *C. albicans* inhibition [4, 55]. This can lead to the release of the 5-methoxysalicylaldehyde in a controlled manner under the *C. albicans* stimuli improving its bioavailability, compared to the free aldehyde in solution which easier can volatilize.

This hypothesis was supported by the investigation of 5-methoxysalicylaldehyde release in a medium mimicking the microbiologic environment (Fig.10). It was observed that the aldehyde was rapidly released during 4 hours, progressively in the next 4 days, reaching then a plateau in line with the establishing of the imination equilibrium. The amount of the released aldehyde over time increased as the crosslinking degree decreased, triggered by the lower concentration of the released aldehyde in the medium, which forced the imination shifting to the reagents.

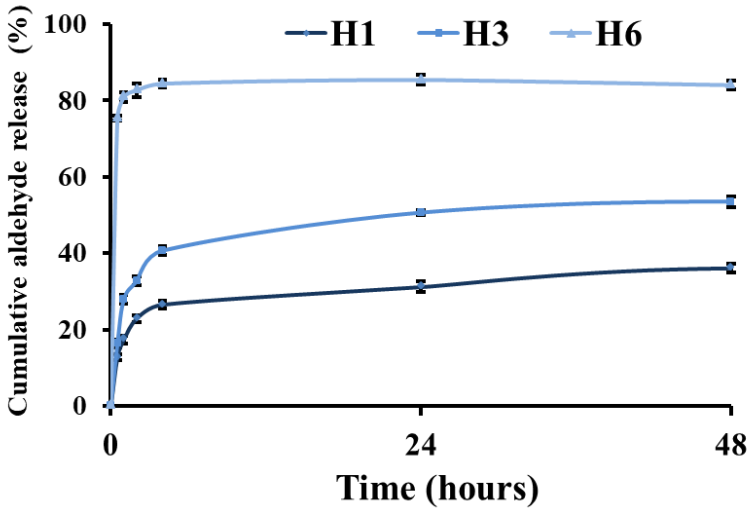

Fig.10. The aldehyde release over 48 hours, at 37°C

3.7. Swelling and stability studies of 5-methoxysalicyl-imine-chitosan hydrogels (Hx)

Swelling and stability at different pHs are important characteristics of hydrogels which can determine their application, especially *in vivo* ones. In this light, the swelling ability and stability of the hydrogels were investigated at three different pHs: 7.4 which is the physiological pH; 5.5 – characteristic for normal dermis, and 8.5 characteristic for infected tissues [4, 56]. As the antimicrobial and biocompatibility tests indicated ***H1.5***, ***H2***, and ***H3*** samples as the most promising for wound healing, they were further investigated (Fig. 11 and Table S4, S5, S6).

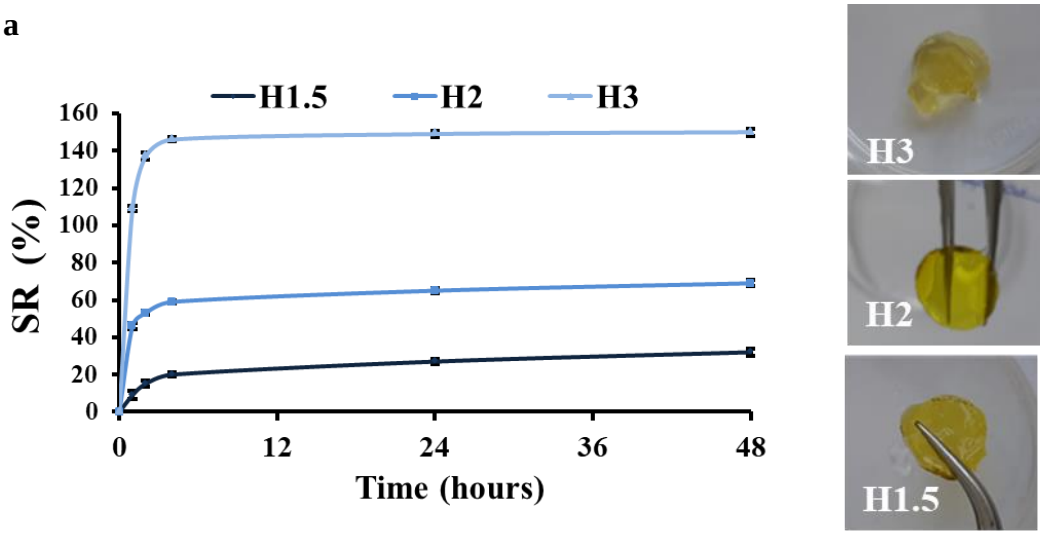

a) **b)**

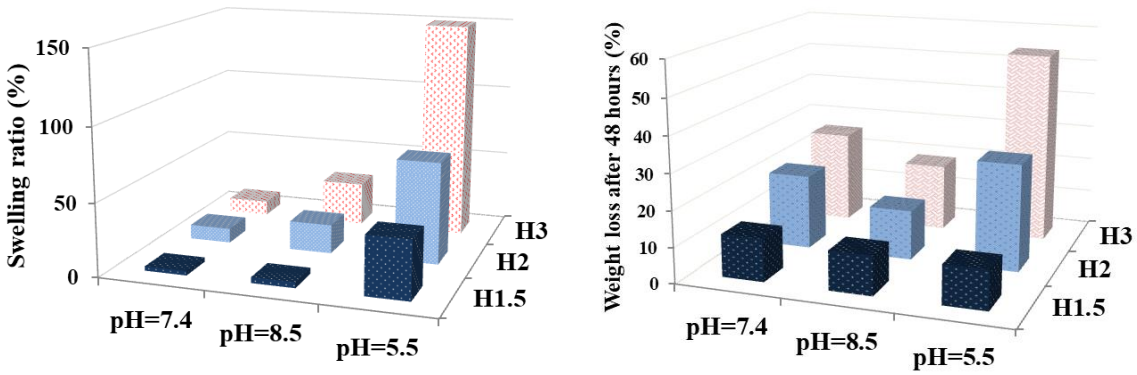

c) **d)**

Fig. 11. The swelling and mass loss of hydrogels investigated in media of different pH, at 37 ^{o}C over 48 hours: a) swelling kinetics in PBS (pH=5.5); b) images of hydrogels after swelling in PBS (pH=5.5); c) the swelling ratio and d) the mass loss, in media of different pH

The hydrogels rapidly swelled in all media and reached the mass equilibrium within 30 minutes (Fig. 11c and Table S4). The swelling ratio increased once the crosslinking density of samples decreased, in line with their morphology; those with lower crosslinking density which presented a loose network of pores and fibers (***H2*** and ***H3***) allowed a higher swelling compared with those with higher crosslinking density which presented interconnected pores (***H1.5***). Comparing the hydrogels' behavior in different pH media, a higher swelling ratio was reached in acidic environment (Fig.11a, b and Table S5). This was explained by the high protonation of free NH_2 groups of chitosan in acidic medium, causing electrostatic repulsions amongst the positive charges and disruption of the H-bonds. Consequently, the network expanded and more water could diffuse into the hydrogel [57]. On the other hand, the higher mass loss at pH=5.5 indicated a greater dissolution due to the hydrolysis of the imine units, which impacted a much loss morphology and consequently an increased swelling (Fig. 11a and b). In media of physiological pH, a slight increase of the swelling ratio was noticed, with insignificant modification of the hydrogel shape. This behavior is in agreement with the deprotonating of free NH_2 groups in basic media, which favored the H-bond interactions and consequently reduced the swelling capacity [17]. Interesting enough, at more basic pH (8.5) the swelling ratio slightly increased.

Regarding the ***hydrogels' stability***, the sample weighting after 2 days showed a higher mass loss for the hydrogels with lower crosslinking degree and it was more advanced in acidic media (Fig. 11d and Table S6). All hydrogels were visual stable in the first 9 days of

experiment, after that, the erosion of the ***H3*** was obvious, while the other samples were visual stable over 3 months of investigation.

3.8. Visual analysis of self-healing properties of the hydrogels

The hydrogelation mechanism of these hydrogels relies on the formation of reversible covalent imine linkages, which are favorable for a self-healing process [10, 20]. Therefore, this possibility was investigated. Firstly, the hydrogels were injectable through a syringe needle and their structure was able to recover after applying a mechanical force. Another approach was to use Rhodamine B to mark one hydrogel, and after that it was injected through a syringe needle on the unmarked hydrogel. It was observed that these two different injected hydrogels were able to connect forming a single piece (Fig. 12). Further, they were mechanical crushed and instantaneous after the mechanical force removing, they formed a single piece again [58]. This behavior points for an easy manipulation at applying on wounds.

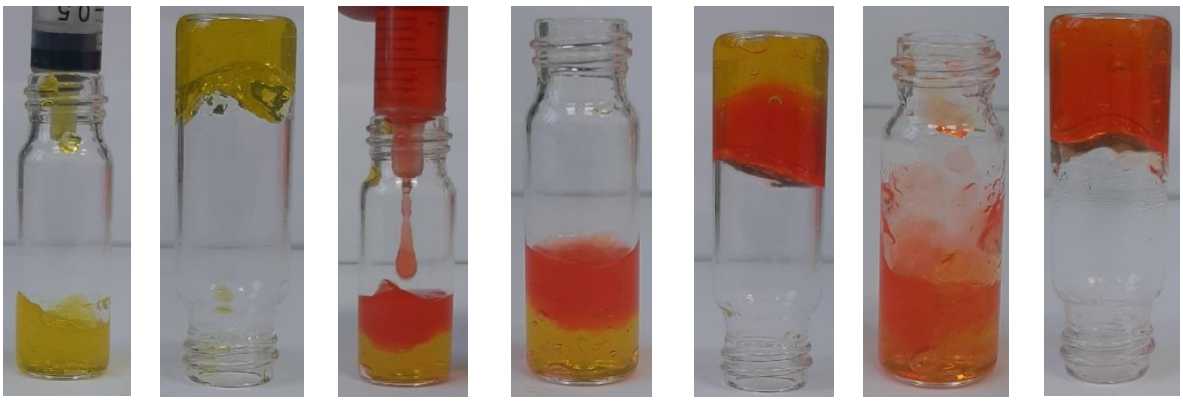

Fig. 12. Visual assessment of the self-healing ability of the hydrogels, exemplified on ***H3***

3.9. In vitro enzymatic biodegradation

The biodegradation behavior of the hydrogels was evaluated in terms of weight loss over a period of 21 days, in conditions mimicking the environment of infected wounds: lysozyme solution of pH 8.5 at 37^{o}C (Fig. 13) [4]. The lysozyme was chosen due to its presence in wound fluid, and its ability to hydrolyze the chitosan into oligomers [59, 60].The most promising samples for *in vivo* applications were chosen for this study (Fig. 13).

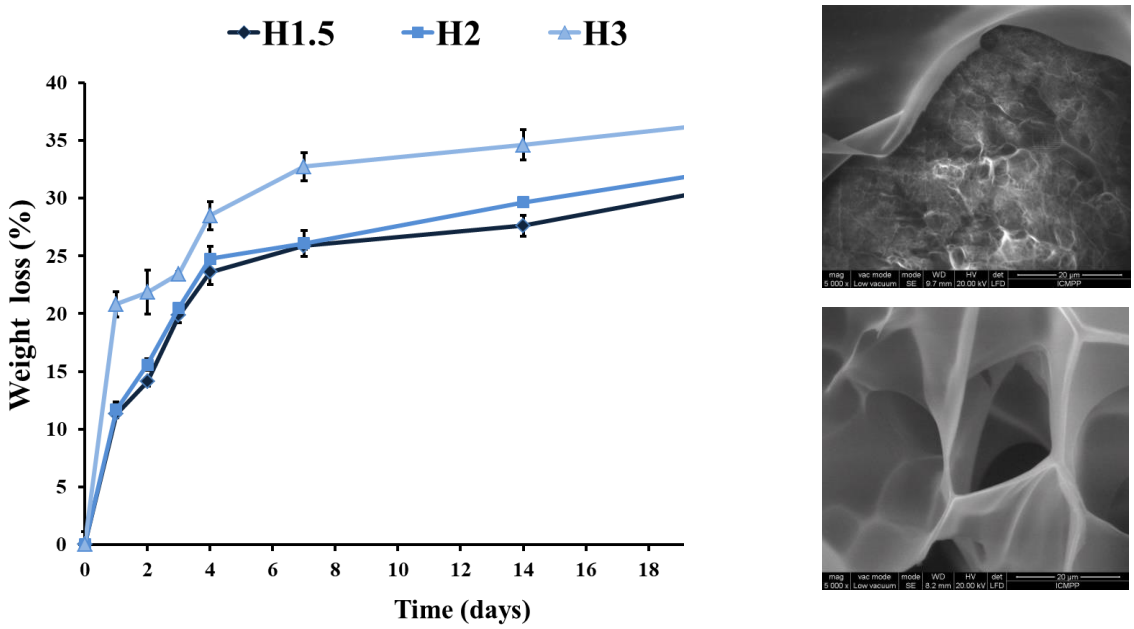

a) **b)**

Fig.13. a) *In vitro* biodegradation profile of representative hydrogels over 21 days. Triplicates of all sample were evaluated (n = 3), and each point shows the mean value ± standard deviation; **b)** images of the hydrogels after degradation

As can be seen in Fig. 13a, the biodegradation occurred in three stages of different degradation rates. Thus, in the first day of investigation, an abrupt mass loss of 11% for ***H1.5*** and ***H2*** and 21% for ***H3*** was recorded (stage I). In the next 3 days, the biodegradation continued in a slower manner, reaching a mass loss around 24% for ***H1.5*** and ***H2*** and 29% for ***H3***, with an average degradation of 6.5 and 3% per day (stage II). Further, in the next 17 days, the rate of mass loss slowed down more at around 0.75% per day, reaching a total mass loss of 31% for ***H1.5*** and ***H2*** and 37% for ***H3*** (stage III). The massive mass loss in the first stage was correlated with the cleavage of the O-C bonds between consecutive N-acetyl-D-glucosamine units catalyzed by lysozyme, leading to chitosan oligomers and their diffusion to the media. The higher biodegradation rate of ***H3*** was attributed to its more porous structure which facilitated the absorption of water and lysozyme into the hydrogel network structure, as its swelling behavior in PBS indicated (swelling rate of 30%, compared to 10% and 4%). Further, in the second biodegradation stage, it is expected as the cleavage of the O-C bonds catalyzed by lysozyme to continue, especially for the ***H1.5*** and ***H2*** samples with slower swelling in basic pH. The higher mass loss of ***H3*** compared to ***H1.5*** and ***H2*** can be also attributed to the hydrolysis of the reversible imine units. This favored the breaking of the crosslinking nodes, weakening the network and thus facilitating the lysozymes to access faster the proper sites. The

slow release in the stage III, could be also affected by the mass loss observed in the swelling investigation. Combining the data from swelling and enzymatic degradation, it can be concluded that the biodegradation of this hydrogels was a result of the lysozyme effect (leading to the cleavage of the O-C bonds) and the erosion by dissolution of the chitosan [60]. The visualization of the hydrogels after degradation showed smaller pores (Figure 13b) indicating a reorganization of the hydrogel during biodegradation, possible due to the formation of new imine units by imination and transamination reactions [38], as the self-healing behavior indicated.

3.10. Conclusions

New natural originating hydrogels with good biocompatibility and antifungal properties were prepared by a simple and easy method from chitosan and a vanillin isomer, i.e. 5-methoxysalicylaldehyde. It was demonstrated that the driving force of hydrogelation rely on the forming of covalent reversible imine bonds and supramolecular organization of the new formed imine units in clusters playing the role of crosslinking nodes. An optimal amount of aldehyde used for chitosan crosslinking generated hydrogels with suitable biocompatibility for medical devices and remarkable antifungal activity. These hydrogels presented porous morphology and consequently good swelling in media mimicking different biologic fluids (e.g. physiological pH, pH of infected tissues and pH of normal dermis) pointing for a good oxygen permeation and exudate drainage. Besides, they were biodegradable and presented self-healing behavior indicating easy manipulation in view of application on skin lesions.

Acknowledgements

The research leading to these results has received funding from the Romanian National Authority for Scientific Research, MEN-UEFISCDI grant, project number RO-NO-2019-0540 (14/2020).

References

[1] X. Zhao, H. Wu, B. Guo, R. Dong, Y. Qiu, P.X. Ma. Antibacterial anti-oxidant electroactive injectable hydrogel as self-healing wound dressing with hemostasis and adhesiveness for cutaneous wound healing, *Biomaterials* 122 (2017) 34–47. https://doi.org/10.1016/j.biomaterials.2017.01.011.

[2] M.A. Matica, F.L. Aachmann, A. Tøndervik, H. Sletta, V. Ostafe. Chitosan as a wound dressing starting material: Antimicrobial properties and mode of action. *Int. J. Mol. Sci.* 20 (2019), 5889. https://doi.org/10.3390/ijms20235889.

[3] P. Hubner, N. Donati, L. Kelin, D.M. Quines, I.C. Tessaro, N.R. Marcilio**.** Gelatin-based films containing clinoptilolite-Ag for application as wound dressing. *Mater. Sci. Eng. C.* 107 (2020) 110215. https://doi.org/10.1016/j.msec.2019.110215.

[4] A. Anisiei, I. Rosca, A.I. Sandu, A. Bele, X. Cheng, L. Marin, Imination of Microporous Chitosan Fibers—A Route to Biomaterials with "On Demand" Antimicrobial Activity and Biodegradation for Wound Dressings, *Pharmaceutics* 14 (2022) 117; https://doi.org/10.3390/pharmaceutics14010117.

[5] J. Su, J. Li, J. Liang, K. Zhang, J. Li. Hydrogel preparation methods and biomaterials for wound dressing. *Life* 11 (2021) 1016. https://doi.org/10.3390/life11101016.

[6] Z. Hussain, H.E. Thu, A.N. Shuid, H. Katas, F. Hussain, Recent advances in polymer-based wound dressings for the treatment of diabetic foot ulcer: An overview of state-of-the-art, *Curr. Drug Targets* 19 (2018) 527–550. https://doi.org/10.2174/1389450118666170704132523.

[7] A. Zhang, Y. Liu, D. Qin, M. Sun, T. Wang, X. Chen, Research status of self-healing hydrogel for wound management: A review, *Int. J. Biol. Macromol*. 164 (2020) 2108–2123. https://doi.org/10.1016/j.ijbiomac.2020.08.

[8] S.P. Ndlovu, K. Ngece, S. Alven, B.A. Aderibigbe. Gelatin-Based Hybrid Scaffolds: Promising Wound Dressings. *Polymers* 13 (2021) 2959. https://doi.org/10.3390/polym13172959.

[9] J. Jagur-Grodzinski, Polymeric gels and hydrogels for biomedical and pharmaceutical applications, *Polym. Adv. Technol.* 21 (2011) 27–47. https://doi.org/10.1002/pat.1504.

[10] Z. Li, Y. Huang, R. Yu, B. Guo, Dual-dynamic-bond cross-linked antibacterial adhesive hydrogel sealants with on-demand removability for post-wound-closure and infected wound healing, *ACS Nano* 15 (2021) 7078–7093. https://doi.org/10.1021/acsnano.1c04206.

[11] T. Dai, M. Tanaka, Y. Huang, M. Hamblin, Chitosan preparations for wounds and burns: Antimicrobial and wound-healing effects, *Expert. Rev. Anti. Infect. Ther*. 9 (2011) 857–879. https://doi.org/10.1586/eri.11.59.

[12] J. Flynn, E. Durack, M. N. Collins, S. P. Hudson, Tuning the strength and swelling of an injectable polysaccharide hydrogel and the subsequent release of a broad spectrum bacteriocin, nisin A, *J. Mater. Chem. B.* 8 (2020) 4029–4038, https://doi.org/10.1039/d0tb00169d.

[13] B.I. Andreica, D. Ailincai, A.I. Sandu, L. Marin, Amphiphilic chitosan-g-poly(trimethylene carbonate) - A new approach for biomaterials design, *Int J Biol Macromol.* 193 (2021) 414–424. https://doi.org/10.1016/j.ijbiomac.2021.10.174.

[14] S. Li, S. Dong, W. Xu, S. Tu, L.Yan, C. Zhao, J. Ding, X. Chen, Antibacterial hydrogels. *Adv. Sci*. 5 (2018) 1700527. https://doi.org/10.1002/advs.201700527.

[15] M. Li, Y. Liang, J. He, H. Zhang, B. Guo, Two-pronged strategy of biomechanically active and biochemically multifunctional hydrogel wound dressing to accelerate wound closure and wound healing, *Chem. Mater*. 32 (2020) 9937–9953. https://dx.doi.org/10.1021/acs.chemmater.0c02823.

[16] Z. Yang, S. Hideyoshi, H. Jiang, Y. Matsumura, J.L. Dziki, S.T. Lopresti, L. Huleihel, G.N.F. Faria, L.C. Fuhrman, R. Lodono. Injectable, porous, biohybrid hydrogels incorporating decellularized tissue components for soft tissue applications. *Acta Biomaterialia* 73 (2018) S1742706118301934. https://doi.org/10.1016/j.actbio.2018.04.003.

[17] R. Rakhshaei, H. Namazi, A potential bioactive wound dressing based on carboxymethyl cellulose/ZnO impregnated MCM-41 nanocomposite hydrogel, *Mater. Sci. Eng. C Mater. Biol.* 73 (2017) 456–464. https://doi.org/10.1016/j.msec.2016.12.097.

[18] X. Qu, A. Wirsen, A.-C. Albertsson, Novel pH-sensitive chitosan hydrogels: swelling behavior and states of water, *Polymer* 41 (2000) 4589–4598. https://doi.org/10.1016/S0032-3861(99)00685-0.

[19] E.A. Kamoun, E.R. Kenawy, X. Chen, A review on polymeric hydrogel membranes for wound dressing applications: PVA-based hydrogel dressings, *J. Adv. Res*. 8 (2017) 217–233. https://doi.org/10.1016/j.jare.2017.01.005.

[20] M.M. Iftime, S. Morariu, L. Marin, Salicyl-imine-chitosan hydrogels: Supramolecular architecturing as a crosslinking method toward multifunctional hydrogels, *Carbohydr. Polym*. 165 (2017) 39–50. https://doi.org/10.1016/j.carbpol.2017.02.027.

[21] L. Marin, D. Ailincai, S. Morariu, L. Tartau-Mititelu, Development of biocompatible glycodynameric hydrogels joining two natural motifs by dynamic constitutional chemistry, *Carbohydr. Polym*. 170 (2017), 60–71. https://doi.org/10.1016/j.carbpol.2017.04.055.

[22] A.M. Olaru, L. Marin, S. Morariu, G. Pricope, M. Pinteala, L. Tartau-Mititelu, Biocompatible based hydrogels for potential application in local tumour therapy, *Carbohydr. Polym*. 179 (2018) 59–70. https://doi.org/10.1016/j.carbpol.2017.09.066.

[23] D. Ailincai, L. Marin, S. Morariu, M. Mares, A.C. Bostanaru, M. Pinteala, B.C.Simionescu, M. Barboiu, Dual crosslinked iminoboronate-chitosan hydrogels with strong antifungal activity against *Candida planktonic* yeasts and biofilms, *Carbohydr. Polym.* 152 (2016) 306–316. https://doi.org/10.1016/j.carbpol.2016.07.007.

[24] M. Iftime, L. Marin, Chiral betulin-imino-chitosan hydrogels by dynamic covalent sonochemistry, *Ultrason. Sonochem*. 45 (2018) 238–247. https://doi.org/10.1016/j.ultsonch.2018.03.022.

[25] L. Marin, S. Moraru, M.C. Popescu, A. Nicolescu, C. Zgardan, B.C. Simionescu, M. Barboiu, Out-of-Water Constitutional Self-Organization of Chitosan-Cinnamaldehyde Dynagels, Chem. Eur. J. 20 (2014) 4814–4821. https://doi.org/10.1002/chem.201304714.

[26] A. Bejan, F. Doroftei, X. Cheng, L. Marin, Phenothiazine-chitosan based eco-adsorbents: A special design for mercury removal and fast naked eye detection, *Int J Biol Macromol.*162 (2020) 1839–1848. https://doi.org/10.1016/j.ijbiomac.2020.07.232

[27] C.W. Li, L. Marin, X.J. Cheng, Chitosan based macromolecular probes for the selective detection and removal of Fe^{3+} ion, *Int. J. Biol. Macromol*. 186 (2021) 303–313. https://doi.org/10.1016/j.ijbiomac.2021.07.044.

[28] A.R. Kumar, V. Nithya, S. Rajeshkumar, S. Gunasekaran et al., An experimental and theoretical evidence for structural and spectroscopic properties of 2-hydroxy-5-methoxybenzaldehyde, *The International Journal of Analytical and Experimental Modal Analysis*. XI (2019)1990-2003. ISSN NO: 0886-9367.

[29] M.M. Iftime, L. Mititelu Tartau, L. Marin, New formulations based on salicyl-imine-chitosan hydrogels for prolonged drug release, *Int. J. Biol. Macromol*. 160 (2020) 398–408. https://doi.org/10.1016/j.ijbiomac.2020.05.207.

[30] X. Wang, P. Xu, Z. Yao, Q. Fang, L. Feng, R. Guo, B. Cheng, Preparation of antimicrobial hyaluronic acid/quaternized chitosan hydrogels for the promotion of seawater-immersion wound healing. *Front. Bioeng. Biotechnol*. 7 (2019) 360. https://doi.org/10.3389/fbioe.2019.00360.

[31] N.A. Mohamed, N.A. Abd El-Ghany, M.M. Abdel-Aziz, Synthesis, characterization, anti-inflammatory and anti-Helicobacter pylori activities of novel benzophenone tetracarboxylimide benzoyl thiourea cross-linked chitosan hydrogels, *Int. J. Biol. Macromol*. 181 (2021) 956–965. https://doi.org/10.1016/j.ijbiomac.2021.04.095.

[32] A.R. Karimi, B. Rostaminejad, L. Rahimi, A. Khodadadi, H. Khanmohammadi, A. Shahriari, Chitosan hydrogels cross-linked with tris(2-(2-formylphenoxy)ethyl) amine: Swelling and drug delivery, *Int. J. Biol. Macromol*. 118 (2018) 1863–1870. https://doi.org/10.1016/j.ijbiomac.2018.07.037.

[33] A.M. Craciun, L. Mititelu-Tartau, G. Gavril, L. Marin. Chitosan crosslinking with pyridoxal 5-phosphate vitamer toward biocompatible hydrogels for *in vivo* applications, *Int. J. Biol. Macromol*. (2021) https://doi.org/10.1016/j.ijbiomac.2021.10.22.

[34] ISO 10993-5:2009 Biological evaluation of medical devices. Part 5: Tests for *in vitro* cytotoxicity. *International Organization for Standardization*, Geneva, Switzerland, 2009.

[35] M. Yildirim-Aksoy, B.H. Beck, Antimicrobial activity of chitosan and a chitosan oligomer against bacterial pathogens of warm water fish, *J. Appl. Microbiol*. 122 (2017) 1570–1578. https://doi.org/10.1111/jam.13460.

[36] Statistical analysis was performed XLSTAT software, Addinsoft, 2021. XLSTAT statistical and data analysis solution. New York, USA. https://www.xlstat.com.

[37] S. Bratskaya, Y. Privar, A. Skatova, A. Slobodyuk, E. Kantemirova, A. Pestov, Carboxyalkylchitosan-based hydrogels with "imine clip": Enhanced stability and amino acids-induced disassembly under physiological conditions. *Carbohydr. Polym*. 274, (2021) 118618. https://doi.org/10.1016/j.carbpol.2021.118618.

[38] P. Kovaricek, J.M. Lehn, Merging constitutional and motional covalent dynamics in reversible imine formation and exchange processes, *J. Am. Chem. Soc*. 134 (2012) 9446–9455. https://doi.org/10.1021/ja302793c.

[39] A. Anisiei, A.C. Bostanaru, M. Mares, L. Marin, Imination of chitosan nanofibers in a heterogeneous system. Synthesis optimization and impact on fiber morphology, Cell. Chem. Technol. 55 (2021), 785–793. https://doi.org/10.35812/CelluloseChemTechnol.2021.55.65.

[40] A.M. Craciun, L. Mititelu Tartau, M. Pinteala, et al., Nitrosalicyl-imine-chitosan hydrogels based drug delivery systems for long term sustained release in local therapy, *J. Colloid Interface Sci*. 536 (2019) 196–207. https://doi.org/10.1016/j.jcis.2018.10.048.

[41] P.D. Chatterjee, M. Pakhira, A.K. Nandi, Fluorescence in "nonfluorescent" polymers, *ACS Omega.* 5 (2020) 30747–30766. https://doi.org/10.1021/acsomega.0c04700.

[42] M. Barón, Definitions of basic terms relating to low-molar-mass and polymer liquid crystals, *Pure Appl. Chem*. 73 (2001) 845–895. http://dx.doi.org/10.1351/pac200173050845.

[43] Estrela dos Santos, E.R. Dockal, É.T.G. Cavalheiro, Thermal behavior of Schiff bases from chitosan, *J. Therm. Anal. Cal*., 79 (2005) 243–248. https://doi.org/10.1007/s10973-005-0042-x.

[44] C.G.T. Netoa, J.A. Giacomettib, A.E. Jobb, F.C. Ferreirab, J.L.C. Fonsecaa, M.R. Pereira, Thermal analysis of chitosan based networks, *Carbohydr. Polym.* 62 (2005) 97–103.

[45] Y. Liang, Z. Li, Y. Huang, R. Yu, B. Guo, Dual-dynamic-bond cross-linked antibacterial adhesive hydrogel sealants with on-demand removability for post-wound- closure and infected wound healing, *ACS Nano* 15 (2021) 7078−7093. https://doi.org/10.1021/acsnano.1c00204.

[46] O.O. Ige, L.E. Umoru, S. Aribo, 2012. Natural products: A minefield of biomaterials. *Int. Sch. Res. Notices*, 983062. https://doi.org/10.5402/2012/983062.

[47] Q. Li, X. Zhu, Vanillin and its derivatives, potential promising antifungal agents, inhibit *Aspergillus flavus* spores via destroying the integrity of cell membrane rather than cell wall, *GOST*, 4 (2021) 54–61. https://doi.org/10.1016/j.gaost.2021.03.002.

[48] E.Y. Jeong, M.Ji Lee, M.S. Kang, H.S. Lee, Antimicrobial agents of 4-methoxysalicylaldehyde isolated from Periploca sepium oil against foodborne bacteria: structure–activity relationship, *Appl. Biol. Chem*. 61 (2018) 397–402. https://doi.org/10.1007/s13765-018-0373-5.

[49] J.H. Kim, K.L. Chan, N. Mahoney, B.C. Campbell, 2011. Antifungal activity of redox-active benzaldehydes that target cellular antioxidation. *Ann. Clin. Microbiol. Antimicrob*. 10, 23. https://doi.org/10.1186/1476-0711-10-23.

[50] S.Y.Y. Wong, I. R. Grant, M. Friedman, C.T. Elliott, C. Situ, Antibacterial activities of naturally occurring compounds against *Mycobacterium avium subsp. paratuberculosis*, *Appl. Environ. Microbiol*. (2008) 5986–5990. https://doi.org/10.1128/AEM.00981-08.

[51] M. Friedman, P.R. Henika, R.E. Mandrell, Antibacterial activities of phenolic benzaldehydes and benzoic acids against *Campylobacter jejuni*, *Escherichia coli*, *Listeria monocytogenes*, and *Salmonella enterica*, *J. Food Prot*. 66 (2003) 10 1811–1821. https://doi.org/10.4315/0362-028X-66.10.1811.

[52] S.P. Chen, G.Z. Wu, D.W. Long, Y.D. Liu, Preparation, characterization and antibacterial activity of chitosan-Ca3V10O28 complex membrane, *Carbohydr. Polym.* 64 (2006) 92–97. https://doi.org/10.1016/j.carbpol.2005.10.024.

[53] R.C. Goy, D. Britto, O.B.G. Assis, A review of the antimicrobial activity of chitosan, *Polímeros* 19 (2009) 241–247. https://doi.org/10.1590/S0104-14282009000300013.

[54] Z. Guo, R. Chen, R. Xing, S. Liu, H. Yu, P. Wang, C. Li, P. Li, Novel derivatives of chitosan and their antifungal activities *in vitro*, *Carbohydr. Res.* 341 (2006) 351–354. https://doi.org/10.1016/j.carres.2005.11.002S.

[55] L. Marin, M. Popa, A. Anisiei, S.A. Irimiciuc, M. Agop, T.C. Petrescu, D. Vasincu, L. Himiniuc, A Theoretical Model for Release Dynamics of an Antifungal Agent Covalently Bonded to the Chitosan, *Molecules* 26 (2021) 2089. https://doi.org/10.3390/molecules26072089.

[56] E. Osti, Skin pH variations from the acute phase to re-epithelialization in burn patients treated with new materials (Burnshield®, semipermeable adhesive film, Dermasilk®, and Hyalomatrix®). Non-invasive preliminary experimental clinical trial, *Ann. Burns Fire Disasters* 21 (2008) 73–77.

[57] G.M.D. Salah Uddin, S. Saha, S. Karmaker, T. Kumar Saha, Adsorption of cefixime trihydrate onto chitosan 10b from aqueous solution: kinetic, equilibrium and thermodynamic studies, *Cellulose Chem. Technol*. 55 (2021) 771-784. https://doi.org/10.35812/CelluloseChemTechnol.2021.55.64.

[58] D. Ailincai, I. Rosca, S. Morariu, L. Mititelu-Tartau, L. Marin. Iminoboronate-chitooligosaccharides hydrogels with strong antimicrobial activity for biomedical applications. *Carbohydr. Polym*. 276 (2022) 118727. https://doi.org/10.1016/j.carbpol.2021.118727.

[59] D.E. Kuehner, J. Engmann, F. Fergg, M. Wernick, H.W. Blanch, J.M. Prausnitz, Lysozyme net charge and ion binding in concentrated aqueous electrolyte solutions, *J. Phys. Chem. B*. 103 (1999) 1368–1374.

[60] S. Hirano, H. Tsuchida, N. Nagao, N-acetylation in chitosan and the rate of its enzymic hydrolysis, *Biomaterials*. 10 (1989) 574–576. https://doi.org/10.1016/0142-9612(89)90066-5.

Graphical Abstract

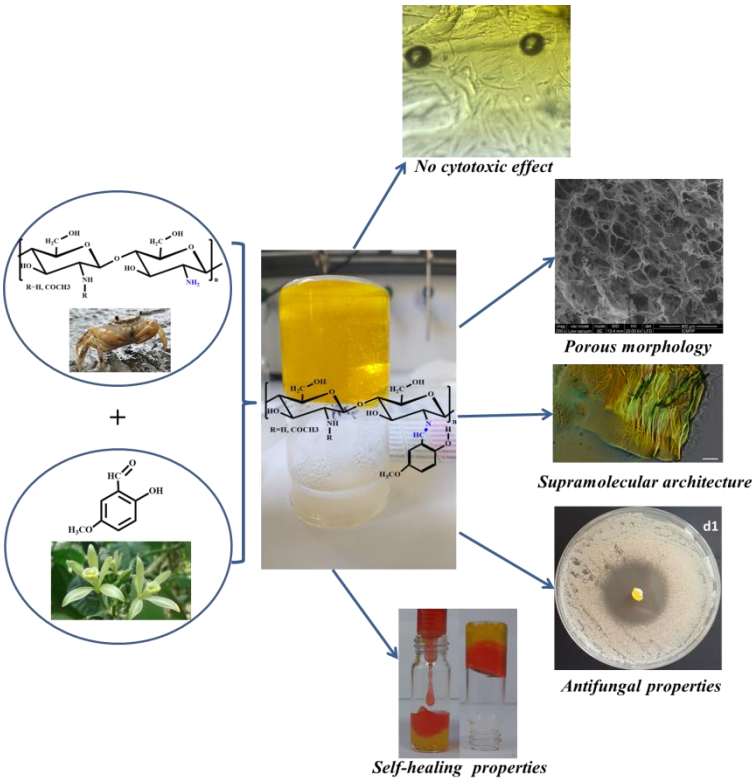
No cytotoxic effect
Porous morphology
Supramolecular architecture
Antifungal properties
Self-healing properties
d1